ISLAMIC UNIVERSITY OF TECHNOLOGY (IUT)

Theoretical Investigation of a Novel GaAs Based Air Slot Nano-Plasmonic Coupler

By

A.B.M RAFID ANWAR (152424)

MD. OMAR SHARIF (152426)

SHADMAN SHAHRIAR MAHMUD (152436)

A Thesis Submitted to the Academic Faculty in Partial Fulfillment of the Requirements for the Degree of

Bachelor of Science in Electrical and Electronic Engineering

Academic Year: 2018-19

Department of Electrical and Electronic Engineering

Islamic University of Technology (IUT)

A Subsidiary Organ of OIC

Gazipur, Dhaka, Bangladesh

November, 2019

Declaration of Authorship

We, A.B.M Rafid Anwar (152424), Md. Omar Sharif (152426) and Shadman Shahriar Mahmud (152436), declare that this thesis titled, 'Theoretical Investigation of a Novel GaAs Based Air Slot Nano-Plasmonic Coupler' and the works presented in it are our own. This work has been done for the partial fulfillment of our Bachelor of Science in Electrical and Electronic Engineering degree and any part of this thesis has not been submitted anywhere else for obtaining any degree.

Submitted By:

_____

A.B.M Rafid Anwar, 152424

_____

Md. Omar Sharif, 152426

_____

Shadman Shahriar Mahmud, 152436

Theoretical Investigation of a Novel GaAs Based Air Slot Nano-Plasmonic Coupler

Approved By:

Dr. Rakibul Hasan Sagor

Thesis Supervisor,

Assistant Professor,

Department of Electrical and Electronic Engineering,

Islamic University of Technology.

Prof. Dr. Md. Ruhul Amin

Head of the Department,

Department of Electrical and Electronic Engineering,

Islamic University of Technology.

Acknowledgements

First and foremost, we offer our gratitude towards Almighty Allah (SWT) for the blessings that allowed us to work in this in sound health.

We are grateful to our research supervisor, Dr. Rakibul Hasan Sagor, for the support and guidance throughout our research at Islamic University of Technology (IUT). From the very beginning of our research journey he was the one paving the way for us and pointing us to our goal. The amount of knowledge and experience he shared with us is beyond value in case of our future works. For all of his helps as our supervisor, we express our heartfelt gratitude towards him.

We would like to thank Md. Saiful Islam Sumon, Lecturer, department of EEE for his help and guidance which allowed us to reach our target. Also, we want to express our gratitude to all the faculty members of the department of EEE, IUT for their inspiration and help.

And last but not the least we are grateful to our family and batchmates for their support and inspiration. Without them it would never have been possible for us to make it this far.

Abstract

A novel rectangular nano-plasmonic coupler based on Gallium Arsenide (GaAs) has been suggested that has an air slot inserted into the dielectric waveguide, considering air as the dielectric material of the metal-dielectric-metal (MDM) plasmonic waveguide. The finite integral technique (FIT) based simulation software which was a commercial software named CST Microwave Studio yielded a coupling efficiency of 81.07% at the wavelength of optical communication i.e. 1.55μm. The most efficient coupling structure has been attained by analyzing the performance with a variety of different dimensions which subsequently results in decent performance over a wide range of wavelengths above the visible spectrum. The elementary flat rectangular composition of the suggested coupler without any tapered edges provides convenience in the manufacturing process, making the coupler affordable and peerless.

Contents

List of Figures

List of Tables:

Abbreviations

ADE	Auxiliary Differential Equation
GaAs	Galium Arsenide
DMD	Dielectric-Metal-Dielectric
FDTD	Finite Difference Time Domain
FIT	Finite Integration Technique
IR	Infra-Red
MDM	Metal-Dielectric-Metal
PML	Perfectly Matched Layer
SPP	Surface Plasmon Polariton
TE	Transverse Electric
TM	Transverse Magnetic

Chapter 1

1. Introduction and Background

1.1 Electrical and Optical Transmission

As time progresses, the world of technology is advancing towards portability and miniaturization, efficiency and lower latency, powerful as well as cheap at the same time. At the root of this endeavors lie modern transistor technology which has reached nano-scale at this point. Using fast transistors in the order of 50nm [1]. has become the norm but the potential performance gains expected with improved scaling is being bottle-necked by the delays associated with the metallic interconnects which communicate digital signals among the transistors. This limitation has now become more evident as the barrier to increasing clock rate has increased higher than ever.

Optical interconnects overcome this barrier with very high and almost loss-less transmission of signals. Unfortunately, miniaturization in this case has not caught up to that of modern electronics, the reason being that optical systems reach a fundamental limit owing to diffraction. When the dimensions of an optical structure (e.g. lens, fibers, optical integrated circuits) becomes close to the wavelength of light, the propagation is obstructed by the occurrence of diffraction. This sets a bar as to what the minimum size of an optical structure should be to avoid this.

1.2 Overcoming the barrier

Using optics as the ideal means of signal transport has not been possible owing to the difference in sizes between the modern electronic and photonic domains. Integrating the optical signals and electric signals onto a single circuit would be the ideal choice. A feasible approach to this ideal is the application of Surface Plasmon Polaritons or SPP in short.

Light can couple to electrons in a metal to form a wave that is bound to its surface. This wave is called SPP. It is characterized by intense fields that decay exponentially away

from the interface between the metal and surrounding environment. This approach has led to the inception of Plasmonics, a new branch of photonics and made possible the localization of electromagnetic energy into nano-scale regions as small as a few nanometers. The wavelength of light poses no notable obstruction here whatsoever.

1.3 SPP and the future

SPP's can be used to design miniaturized opto-electronic circuits with subwavelength components or so it may seem. There still remains a problem with propagation distance of the SPP because of the large absorption inherent to metals. Therefore, the challenge lies in mitigating the losses while leveraging the unique properties of SPP.

Various types of metallic nano-structures have been proposed for guiding SPP modes with the goal of reducing losses. These include tapered form [2], silver nano-wire based [3], Si-based [4], MDM based [5] and so on. Not all of the proposed structures have achieved the same kind of localization nor have they mitigated losses as desired. Among the proposed structures, the Metal-Dielectric-Metal waveguide shows much potential due to it being capable of guiding optical signals in sub-wavelength scale through Surface plasmons [6]. A novel idea is using dielectric waveguide along with the MDM plasmonic waveguide. Transmission through long distances with low losses is achieved by using the dielectric whereas the MDM is used for handling the subwavelength scaling of the light signals for use in opto-electronic devices. This calls for efficient coupling between the two types of waveguides for the best results.

Couplers of different forms and structures are used to facilitate coupling. The higher the transmission efficiency, the better the coupler. Maximizing the efficiency has been the present challenges in Plasmonics. Research is still going to introduce new structures and further optimize the existing ones in order to achieve better results.

1.4 Literature Review

Plasmonics harbor lots of potential for exploration and research. Originating in the ninety's plasmonics have gained the interest of researchers for the endless list of

possibilities for improvement it can provide in fields like cancer treatment [7], photovoltaic devices [8],chemical and biological sensing [29], super lensing [9] and many more. We have come to know from the research work of Harry A. Atwaterand and Albert Polman where it was stated that Plasmonics improves absorption in Photovoltaic devices [10]. How perfect imaging is possible through a flat thin metal film has been shown by Satoshi Kawata, Yasushi Inouye and Prabhat Verma. It was also discovered that light absorption in thin solar cell can be increased by scattering from the metal nano-particles near their localized surface plasmons. This causes an increase in photocurrent in solar cells [30]. Harry A. Atwater noted that plasmon resonance absorption can be used to kill cancer cells. This literature review mainly focuses on Surface Plasmon Polaritons (SPP), waveguides and couplers which has been the primary focus of Plasmonics in today's times.

In the 1980s it was experimentally discovered by researchers that, under the right circumstances, directing light waves at the interface between a metal and a dielectric material can induce a resonant interaction between the waves and the mobile electrons at the interface. The oscillations of electrons had matched those of the electromagnetic field incident on the metal. This resulted in generation of surface plasmons--density waves of electrons that propagate along the interface like the ripples that spread across the surface of a pond after a stone is thrown in it. Researchers have found that they can produce surface plasmons with the same frequency as the current electromagnetic waves but with a much shorter wavelength by creatively designing the metal-dielectric interface. This phenomenon could allow the plasmons to carry information from one part of a microprocessor to another through nanoscale wires called interconnects. Such interconnects would be a great news for chip designers who have had a harder time building minute electronic circuits that can move data quickly across the chip despite using the smallest and fastest of transistors.

Different waveguide designs for transporting SPP have been proposed in the studies of different researchers. It has been reported to our knowledge that Mark I. In 2004 Stockman predicts in his research that SPP are slowed down as they arrive at the tip of a tapered plasmonic waveguide[2]. In 2006 R. Steinberger et.al. notified that using $Si0_2$ on gold stripes in the waveguide provides large effective refractive index[31]. In 2008 Anna L. Pyayt et.al proposed the integration of multiple silver nanowire plasmonic waveguides with polymer optical waveguides for the nanoscale confinement and

guiding of light on a chip [3]. Oulton RF discovered that a waveguide which uses metal as well as low index and high index dielectric material allowed for longer propagation distances while providing the same degree of confinement[32]. In 2009 Changjun Min et.al. in his study showed how MDM waveguides can perform better in tunneling SPP modes compared to most other waveguides [4]. In 2010 Alexey V. Krasavin et.al. mentioned that the high refractive index of Si assures strong confinement and a very high level of photonic integration in the Si-based waveguide that he studied [5].

Sub-wavelength scale opto-electric circuits require coupling between dielectric waveguides and the plasmonic waveguides. The dielectric waveguides transmit optical signals and the plasmonics waveguides carry SPP modes. Good integration is achieved when the coupler transmits the light signals to the plasmonic waveguide efficiently. Therefore, designing efficient nano-plasmonic couplers with different materials and structures has been the endeavor of researchers. Saiful Islam et.al. put forward a compact nano-plasmonic coupler of semi-elliptical form. Waveguide having a tapered gap for adiabatic and nonadiabatic coupling was suggested by D.Pile. A theory of a coupler with λ/4 impedance matching was shown in detail by Pavel Ginzberg[33]. In 2019 Rakibul Hasan et.al. stated a study of semi-elliptical structured coupler having air gaps. A coupler optimized with multisection tapers was designed by G.Veronis.

1.5 Thesis Objective

The objective of the study is designing a coupler which has high transmission efficiency so that it can facilitate better coupling between dielectric and plasmonic coupler. This goal is fulfilled in the following order:

- Choosing materials that are better suited for the purpose by reviewing properties of different materials.
- Choosing a suitable coupler structure by reviewing structures proposed by different researchers.
- Implementing the coupler in the design environment of CST.
- Assessing the performance of the coupler and optimizing it using the simulation tools of CST for achieving better efficiency.

- Summarizing important conclusions from the obtained results and discussing potential applications for the future.

1.6 Thesis Organization

This Thesis book has been arranged in the following way:

- Chapter 2 describes the background of SPP, its definition and why it is necessary. It also tells about the underlying theory behind the propagation of SPP.
- Chapter 3 explains the Finite Difference Time Domain (FDTD) method which is a robust tool for solving Maxwell equations and is essential if simulation of the coupler is performed manually using MATLAB.
- Chapter 4 discusses the theoretical background of a coupler. It also contains elaborate details of the proposed structure and how it reached the final design.
- Chapter 5 lays down the performance analysis of the proposed structure through graphical and tabular representation.
- Chapter 6 tells about the concluding remarks of the proposed structure and the potential activities for the future.

Chapter 2

2. SPP Propagation Theory

2.1 Introduction to SPP

Surface Plasmon Polariton or SPP in short is an electromagnetic wave that generates and propagates along the interface of a metal and a dielectric. Under the right conditions, when light incidents on the surface of a metal, the oscillation of the mobile electrons at the surface match those of the incident field. This results in a wave of electrons moving along the surface of the metal.

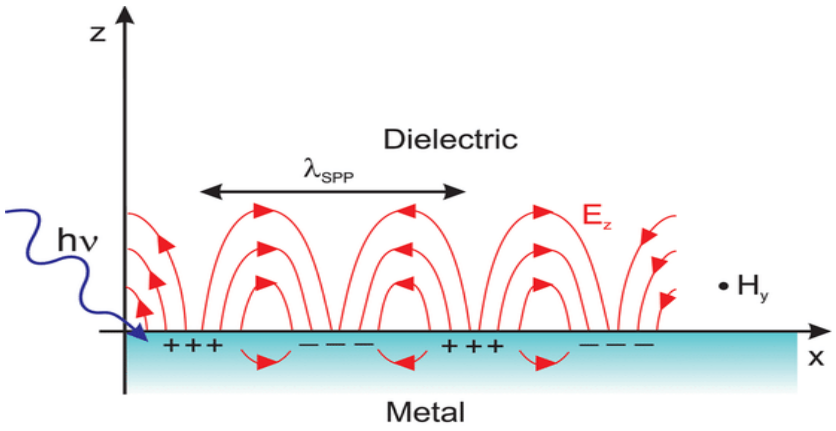

Figure 2.1: Schematic illustration of electromagnetic wave and surface charges at the interface between the metal and the dielectric material [34].

These plasmons are characterized by intense fields which decline exponentially from the interface between metal and dielectric. Strongly enhanced local fields, tremendous sensitivity to changes in the local environment and the ability to localize energy to tiny volumes not restricted by the wavelength of the exciting light are important features that the Surface plasmons possess.

2.2 Impact of SPP

Plasmons have found a wide range of applications in different fields of science due to their unique properties. In the fields of chemistry and biology the sensitivity of surface

plasmons is used as the basis for strong chemical and biochemical detectors capable of monitoring molecular binding events. The large field strengths of surface plasmons is useful in optics for enhancing a variety of phenomena like Raman scattering and light transmission through sub-wavelength apertures. The sensitivity of SPP raises the probability of enhancing the performance of modulators, switches and chip-scale optical sensors. The size of certain SPP configurations smaller than the operation wavelength offers a path to decrease the size of components of optical systems beyond the diffraction limit.

2.3 Using SPP to tackle Diffraction limit

The diffraction limit is imposed on the propagation of light preventing it to transmit properly through optical systems of size less than half of its wavelength. Using materials with negative dielectric permittivity is one of the most feasible ways of circumventing the diffraction limit and achieving localization of electromagnetic energy (at optical frequencies) into nanoscale regions as small as a few nanometers [11]. Metals below the plasma frequency can readily serve this purpose. Surface plasmon–polariton (SPP) modes are EM waves coupled to collective oscillations of electron plasma in the metal and move along the interfaces of metal and dielectric.

It has been known for decades that there exists surface plasmon–polariton waves, that are localized near and propagate along the interface of a plasma like medium. But this area of research gained rapid attention when scientists realized that SPP modes in nano-metallic structures can unlock the way for localizing guided light signals way beyond the diffraction limit for EM waves in dielectric media. Thus, visible and infrared light can be concentrated into small regions of a few nanometers and depends only on the atomic structure of matter, dissipation and the spatial dispersion of light. By proper designing of the metal-dielectric interface it can be made to generate surface plasmons with the same frequency as the outside electromagnetic waves but with a much shorter wavelength. This could allow the surface plasmons to travel along nanoscale interconnects, carrying information from one place to another.

Thus, SPP is the key to designing smaller circuits at the same scale as modern transistors but with faster transmission speeds.

2.4 Propagation of SPP

The interaction of metals with electromagnetic fields can be very well described by Maxwell's equations. Even metallic nanostructures down to sizes on the order of a few nanometers can be described without a need to resort to quantum mechanics. Surface plasmons are electromagnetic waves that propagate along the interface of metal-dielectric as a result of excitation of electrons. Thus, Maxwell's equations are at the root of the propagation of Surface Plasmons.

2.5 The Maxwell's Equations

Maxwell's equations for macroscopic electromagnetism are in the following form:

From Gauss's Law for electric field: $\vec{\nabla}.\vec{D} = \rho_{ext}.$ (2.1)

From Gauss's Law for magnetic field: $\vec{\nabla}.\vec{B} = 0.$ (2.2)

From Faraday's Law: $\vec{\nabla} \times \vec{E} = -\frac{\partial \vec{B}}{\partial t}.$ (2.3)

From Ampere's Law: $\vec{\nabla} \times \vec{H} = J_{ext} + \frac{\partial \vec{D}}{\partial t}.$ (2.4)

Here, $\vec{E}$ is the electric field vector in volt per meter,

$\vec{D}$ is the electric flux density vector in coulombs per square meter,

$\vec{H}$ is the magnetic field vector in amperes per meter,

$\vec{B}$ is the magnetic flux density vector in webbers per square meter,

ρ_{ext} is the charge density,

J_{ext} is the current density.

These four equations thus link the four macroscopic fields $\vec{D}$, $\vec{E}$, $\vec{H}$ and $\vec{B}$ with the external charge and current densities ρ_{ext} and J_{ext}.

The four macroscopic fields can be also linked further via the polarization $\vec{P}$ and magnetization $\vec{M}$ by:

$$\vec{D} = \varepsilon_0 \vec{E} + \vec{P}\,. \tag{2.5}$$

$$\vec{H} = \frac{1}{\mu_0}\vec{B} - \vec{M}. \tag{2.6}$$

For linear, isotropic and non-magnetic media we get the following constitutive relations:

$$\vec{D} = \varepsilon_0 \varepsilon_r \vec{E}. \tag{2.7}$$

$$\vec{B} = \mu_0 \mu_r \vec{H}. \tag{2.8}$$

Here, ε_0 is electric permittivity of vacuum in Farad per meter,

ε_r is the relative permittivity,

μ_0 is the magnetic permeability of vacuum in Henry per meter,

μ_r is the relative permeability.

Combining the curl equations leads to the wave equation:

$$\vec{\nabla} \times \vec{\nabla} \times \vec{E} = -\mu_0 \frac{\partial^2 \vec{D}}{\partial t^2}\,, \tag{2.9}$$

$$\vec{K}\left(\vec{K} \cdot \vec{E}\right) - K^2 \vec{E} = -\varepsilon(K, \omega)\frac{\omega^2}{c^2}\vec{E}. \tag{2.10}$$

The Electromagnetic Wave Equation:

In the absence of external charge, the curl equations can be combined to yield:

$$\vec{\nabla} \times \vec{\nabla} \times \vec{E} = -\mu_0 \frac{\partial^2 \vec{D}}{\partial t^2}. \tag{2,.11}$$

We have the identities,

$$\vec{\nabla} \times \vec{\nabla} \times \vec{E} = \vec{\nabla}(\vec{\nabla} \cdot \vec{E}) - \nabla^2 \vec{E} \text{ and} \tag{2.12}$$

$$\vec{\nabla} \cdot (\varepsilon \vec{E}) = \vec{E} \cdot \vec{\nabla}\varepsilon + \vec{\nabla} \cdot \vec{E}. \tag{2.13}$$

Using these the above equation can be rewritten as

$$\vec{\nabla}\left(-\frac{1}{\varepsilon}\vec{E} \cdot \nabla\varepsilon\right) - \nabla^2 \vec{E} = -\mu_0 \varepsilon_0 \varepsilon \frac{\partial^2 \vec{E}}{\partial t^2}\,. \tag{2.14}$$

For negligible variation of the dielectric profile ε = ε(r) over distances on the order of one optical wavelength, the equation simplifies to the central equation of electromagnetic wave theory:

$$\nabla^2\vec{E} - \frac{\varepsilon}{C^2}\frac{\partial^2\vec{E}}{\partial t^2} = 0\ . \qquad (2.15)$$

Here, $C = \frac{1}{\sqrt{\mu_0\,\varepsilon_0}}$ velocity of light

In a progression of two steps, (2.15) is made into a form suitable for describing confined propagating waves. A harmonic time dependence of the electric field $E(r,t) = E(r)e^{-i\omega t}$ is assumed at first. Inserting the assumption into the equation we get:

$$\nabla^2 E + K_0^2\varepsilon E = 0. \qquad (2.16)$$

Here, $K_0 = \frac{\omega}{C}$ is the wave vector of the propagating wave in vacuum.

The equation is known as the Hemholtz equation.

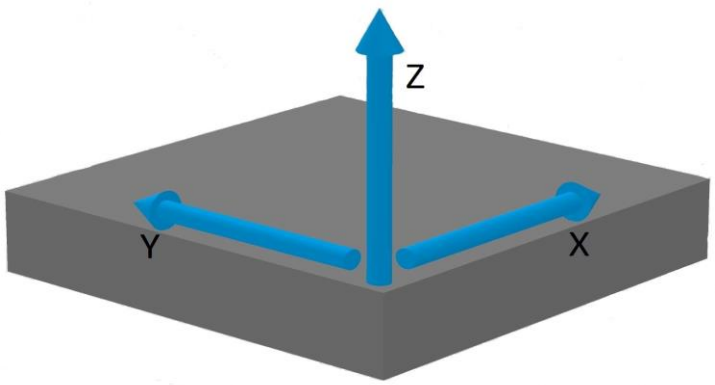

Figure 2.2: Typical planar waveguide geometry. The waves propagate along the x-direction in a cartesian coordinate system.

For simplicity change of ε with respect to only on one spatial coordinate is considered. So spatial variation is seen along the x-direction of a cartesian coordinate system whereas there is no spatial variation in the perpendicular, in-plane y-direction (see Fig. 2.2); therefore ε = ε(z). Applied to electromagnetic surface problems, the plane z = 0 coincides with the interface sustaining the propagating waves, which can now be described as $\vec{E}(x,y,z) = \vec{E}(z)e^{j\beta x}$. β=kx is called the propagation constant of the traveling wave. It is a complex number and corresponds to the component of the wave vector in the direction of propagation.

Inserting this expression into the Hemholtz equation we get,

$$\frac{\partial^2 E(z)}{\partial z^2} + (K_0^2\varepsilon - \beta^2)E = 0\ . \qquad (2.17)$$

Naturally, a similar equation exists for the magnetic field $\vec{H}$.

The field $\vec{E}$ and $\vec{H}$ can be decomposed in cartesian co-ordinate system as

$$\vec{E} = E_x.\vec{a}_x + E_y.\vec{a}_y + E_z.\vec{a}_z\ , \tag{2.18}$$

$$\vec{H} = H_x.\vec{a}_x + H_y.\vec{a}_y + H_z.\vec{a}_z\ . \tag{2.19}$$

For Harmonic time dependence $\frac{\partial}{\partial t} = -j\omega$ the following set of coupled equations are obtained:

$$\frac{\partial E_z}{\partial y} - \frac{\partial E_y}{\partial z} = j\omega\mu_0 H_x\ , \tag{2.20}$$

$$\frac{\partial E_x}{\partial z} - \frac{\partial E_z}{\partial x} = j\omega\mu_0 H_y\ , \tag{2.21}$$

$$\frac{\partial E_y}{\partial x} - \frac{\partial E_x}{\partial y} = j\omega\mu_0 H_z\ , \tag{2.22}$$

$$\frac{\partial Hz}{\partial y} - \frac{\partial H_y}{\partial z} = j\omega\varepsilon_0\,\varepsilon E_x\ , \tag{2.23}$$

$$\frac{\partial Hx}{\partial z} - \frac{\partial H_z}{\partial x} = j\omega\varepsilon_0\,\varepsilon E_y\ , \tag{2.24}$$

$$\frac{\partial Hy}{\partial x} - \frac{\partial H_x}{\partial y} = j\omega\varepsilon_0\,\varepsilon E_z\ . \tag{2.25}$$

For propagation is in x-direction $\frac{\partial}{\partial x} = -j\beta$, and homogeneity in y- direction $\frac{\partial}{\partial y} = 0$. So the equations can be simplified as:

$$-\frac{\partial E_y}{\partial z} = j\omega\mu_0 H_x\ , \tag{2.26}$$

$$\frac{\partial E_x}{\partial z} - j\beta E_z = j\omega\mu_0 H_y\ , \tag{2.27}$$

$$j\beta E_y = j\omega\mu_0 H_z\ , \tag{2.28}$$

$$\frac{\partial H_y}{\partial z} = j\omega\varepsilon_0\,\varepsilon E_x\ , \tag{2.29}$$

$$\frac{\partial \mathrm{Hx}}{\partial z} - \mathrm{j}\beta \mathrm{H_z} = \mathrm{j}\omega\varepsilon_0\,\varepsilon \mathrm{E_y}\,, \tag{2.30}$$

$$\mathrm{j}\beta \mathrm{H_y} = \mathrm{j}\omega\varepsilon_0\,\varepsilon \mathrm{E_z}\,. \tag{2.31}$$

There are two sets of self-consistent solutions for the propagating waves and have different polarization properties. The first set are the transverse magnetic (TM or p) modes, where only the field components E_x, E_z and H_y are nonzero, and the second set the transverse electric (TE or s) modes, with only H_x, H_z and E_y being nonzero.
For TM modes, the system of governing equations reduces to:

$$\mathrm{E_x} = -\mathrm{j}\frac{1}{\omega\varepsilon_0\,\varepsilon}\frac{\partial \mathrm{H_y}}{\partial z}\,, \tag{2.32}$$

$$\mathrm{E_z} = -\beta\frac{1}{\omega\varepsilon_0\,\varepsilon}\mathrm{H_y}\,. \tag{2.33}$$

Therefore, the wave equation for TM Polarized wave will be

$$\frac{\partial^2 \mathrm{H_y}}{\partial z^2} + (\mathrm{K_0^2}\varepsilon - \beta^2)\mathrm{H_y} = 0\,, \tag{2.34}$$

Similarly the TE polarized equations will be

$$\mathrm{H_x} = \mathrm{j}\frac{1}{\omega\mu_0}\frac{\partial \mathrm{E_y}}{\partial z}\,, \tag{2.35}$$

$$\mathrm{H_z} = \beta\frac{1}{\omega\mu_0}\mathrm{E_y}\,. \tag{2.36}$$

And the corresponding TE wave equation will be

$$\frac{\partial^2 \mathrm{E_y}}{\partial z^2} + (\mathrm{K_0^2}\varepsilon - \beta^2)\mathrm{E_y} = 0\,. \tag{2.37}$$

2.6 Surface Plasmon Polaritons at a single interface

A single, flat interface between a dielectric, non-absorbing half-space($z> 0$) with positive real dielectric constant ε^2 and an adjacent conducting half space ($z< 0$)

described via a dielectric function $\varepsilon^1(\omega)$ can be considered for sustaining the propagation of SPP.

Figure 2.3: SPP at the Single interface.

The TM solutions:

$$H_y(z) = A_2 e^{ibx} e^{-k_2 z}\,, \tag{2.37}$$

$$E_x(z) = iA_2 \frac{1}{\omega\varepsilon_0 \varepsilon_2} k_2 e^{ibx} e^{-k_2 z}, \tag{2.38}$$

$$E_z(z) = -A_1 \frac{\beta}{\omega\varepsilon_0 \varepsilon_2} e^{ibx} e^{-k_2 z}\,. \tag{2.39}$$

For z>0,

$$H_z(z) = A_2 e^{j\beta x} e^{-k_2 z}\,, \tag{2.40}$$

$$E_x(z) = jA_2 \frac{1}{\omega\varepsilon_0 \varepsilon_2} k_2 e^{j\beta x} e^{-k_2 z}, \tag{2.41}$$

$$E_z(z) = -A_1 \frac{\beta}{\omega\varepsilon_0 \varepsilon_2} e^{j\beta x} e^{-k_2 z}\,. \tag{2.42}$$

For z<0,

$$H_y(z) = A_1 e^{j\beta x} e^{k_1 z}\,, \tag{2.43}$$

$$E_x(z) = -jA_1 \frac{1}{\omega\varepsilon_0 \varepsilon_1} k_1 e^{j\beta x} e^{k_1 z}\,, \tag{2.44}$$

$$E_x(z) = -A_1 \frac{\beta}{\omega\varepsilon_0 \varepsilon_1} e^{j\beta x} e^{-k_1 z}\,. \tag{2.45}$$

The continuity of H_y and $\varepsilon_i E_z$ at the metal dielectric interface requires

$$A_1 = A_2 \text{ and} \tag{2.46}$$

$$\frac{k_2}{k_1} = -\frac{\varepsilon_2}{\varepsilon_1}\,. \tag{2.47}$$

The surface wave exists at the metal dielectric interface with opposite sign of their real

dielectric permittivities. Thus, we can write:

$$k_1^2\varepsilon = \beta^2 - k_0^2\varepsilon_1 \,, \tag{2.48}$$

$$k_2^2\varepsilon = \beta^2 - k_0^2\varepsilon_2 \,. \tag{2.49}$$

Combining this and (2.12) we arrive at the central result of this section, the dispersion relation of SPPs propagating at the interface between the two half spaces:

$$\beta = k_0\sqrt{\frac{\varepsilon_1\varepsilon_2}{\varepsilon_1+\varepsilon_2}} \tag{2.50}$$

The TE surface modes can be expressed as

$$E_y(z) = A_2 e^{j\beta x} e^{-k_2 z} \,, \tag{2.51}$$

$$H_x(z) = -jA_2\frac{\beta}{\omega\mu_0}k_2 e^{j\beta x} e^{-k_2 z} \,, \tag{2.52}$$

$$H_z(z) = -A_2\frac{\beta}{\omega\mu_0}k_2 e^{j\beta x} e^{-k_2 z}. \tag{2.53}$$

for $z > 0$, and

$$E_y(z) = A_1 e^{j\beta x} e^{-k_1 z} \,, \tag{2.54}$$

$$H_x(z) = jA_1\frac{\beta}{\omega\varepsilon_0\,\varepsilon_1}k_1 e^{j\beta x} e^{k_1 z} \,, \tag{2.55}$$

$$H_z(z) = A_1\frac{\beta}{\omega\varepsilon_0\,\varepsilon_1}k_2 e^{j\beta x} e^{k_1 z} \,. \tag{2.56}$$

Continuity of Ey and Hx at the interface leads to the condition

$$A_1\,(k_1 + k_2) = 0 \tag{2.57}$$

This condition is only fulfilled if $A_1 = 0$, so that also $A_2 = A_1 = 0$. Thus, no surface modes exist for TE polarization. Surface plasmon polaritons only exist for TM polarization.

2.7 SPP at Double Interfaces

Examples of double interface setups are MDM or Metal-Dielectric-Metal and DMD or Dielectric-Metal-Dielectric. In such cases, SPPs are formed at both the interfaces. When the distance is shorter than decay distance, it forms coupled mode of SPP. This

coupled mode of propagation can also be sub-divided into even and odd modes, as shown in the figure:

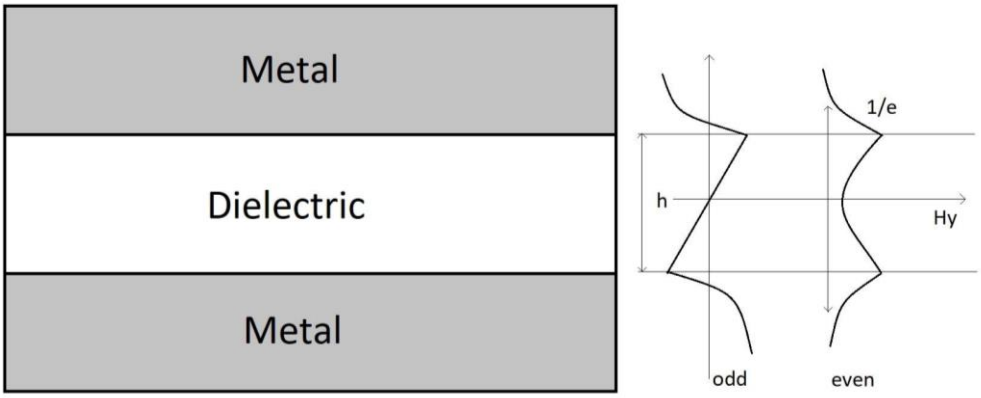

Figure 2.4 : Propagation of SPP at dual interface.

Chapter 3

3. Overview of Finite-Difference Time-Domain Method

3.1 Introduction

The Finite-Difference Time-Domain method (FDTD) is one of the most robust tool for the solution of electromagnetic problems. It has been successfully applied to a wide range of problems, such as the dispersion of metal objects and dielectrics, antennas and electrical absorption in the radiation-exposed to human body. This method is comparatively easier than other methods to calculate electromagnetic field. It has been applied for three dimensional programming for visualizing electric and magnetic fields. The technique was first proposed by K. Yee and then in 1975 Taflove and Brodwin obtained the numerical stability criterion for Yee's algorithm [12]. For solving an electromagnetic problem, the idea is to simply discretize the Maxwell's equations with approximations of central difference, both in time and space.

FDTD method is classified into three simulations. These simulation methods are used for one dimension, two dimension and also three dimensions [13]. Thus, the simulations are called:

1. One dimensional simulation (1D)
2. Two dimensional simulation (2D)
3. Three dimensional simulation (3D)

For Linear, isotropic and non-dispersive materials, The Maxwell's equations are:

$$\nabla \times \vec{H} = \frac{\partial \vec{D}}{\partial t} \tag{3.1}$$

$$\nabla \times \vec{E} = -\frac{\partial \vec{B}}{\partial t} \tag{3.2}$$

$$\nabla \cdot \vec{B} = 0 \tag{3.3}$$

$$\nabla \cdot \vec{D} = \rho \tag{3.4}$$

The Maxwell's differential equation can be determined by the change in electric field $\vec{E}$ in time which is dependent on the change in magnetic field $\vec{H}$ in space. Again, the change in magnetic field $\vec{H}$ in time, is dependent on the change in electric field $\vec{E}$ in space.

3.2 The Yee Algorithm

The algorithm used in FDTD simulations is known as the Yee algorithm. The originality of the idea of Yee resides in the allocation in space of the electric and magnetic field component. Yee's grid can be applied for one dimension, two dimension and also three dimension to calculate electric field and magnetic field. To visualize the Yee's grid, here we are looking for one dimensional Yee's grid [14]. First of all, it assigns the computational region as physical region with the one we are working. Then it discretizes the volume into cells in Cartesian coordinates to solve electric and magnetic field numerically.

The method is used within two of Maxwell's equations:

$$D\frac{\partial \vec{H}}{\partial t} = -\frac{1}{\mu}\nabla \times \vec{E} \tag{3.5}$$

$$D\frac{\partial \vec{E}}{\partial t} = \frac{1}{\varepsilon}\nabla \times \vec{H} \tag{3.6}$$

For linear, isotropic and non-magnetic media we get the following constitutive relations that are used to calculate $\vec{E}$ field and $\vec{H}$ field.

$$D = \varepsilon_0 \varepsilon_r \tag{3.7}$$

$$B = \mu_0 \mu_r \vec{H} \tag{3.8}$$

These constitutive relations help to shift $\vec{E}$ field to $\vec{H}$ field and $\vec{H}$ field to $\vec{E}$ field.

The curl of Maxwell's equation is converted into time domain and space domain and they are coupled scalar first order differential equation given in Cartesian coordinates. The curl operation of equation become:

$$\frac{\partial E_z}{\partial y} - \frac{\partial E_y}{\partial z} = \mu \frac{\partial H_x}{\partial t} \tag{3.9}$$

$$\frac{\partial E_x}{\partial z} - \frac{\partial E_z}{\partial x} = \mu \frac{\partial H_z}{\partial t} \tag{3.10}$$

$$\frac{\partial E_y}{\partial x} - \frac{\partial E_x}{\partial y} = \mu \frac{\partial H_z}{\partial t} \tag{3.11}$$

$$\frac{\partial Hz}{\partial y} - \frac{\partial H_y}{\partial z} = \varepsilon \frac{\partial E_x}{\partial t} \tag{3.12}$$

$$\frac{\partial Hx}{\partial z} - \frac{\partial H_z}{\partial x} = \varepsilon \frac{\partial E_y}{\partial t} \tag{3.13}$$

$$\frac{\partial Hy}{\partial x} - \frac{\partial H_x}{\partial y} = \varepsilon \frac{\partial E_z}{\partial t} \tag{3.14}$$

We take $\vec{E}$ and $\vec{H}$ in time so that $\vec{E}$ exists at integer time steps (0, t, 2Δt, …) and $\vec{H}$ exists at half time steps (Δt/2, t+ Δt/2, 2t+ Δt/2,…).

$$\nabla \times \vec{E}\big|_t \cong -\mu \frac{\vec{H}\big|_{t+\frac{\Delta t}{2}} - \vec{H}\big|_{t-\frac{\Delta t}{2}}}{\Delta t} \tag{3.15}$$

$$\nabla \times \vec{H}\big|_{t+\frac{\Delta t}{2}} \cong \varepsilon \frac{\vec{E}\big|_{t+\Delta t} - \vec{E}\big|_t}{\Delta t} \tag{3.16}$$

For our convenience, one dimensional simulation (1D) is used to solve electromagnetic problem. The way 1D works is explained elaborately in fig. 3.1.

Each field component depends on the field of previous time step itself and the surrounding component in Yee's algorithm.

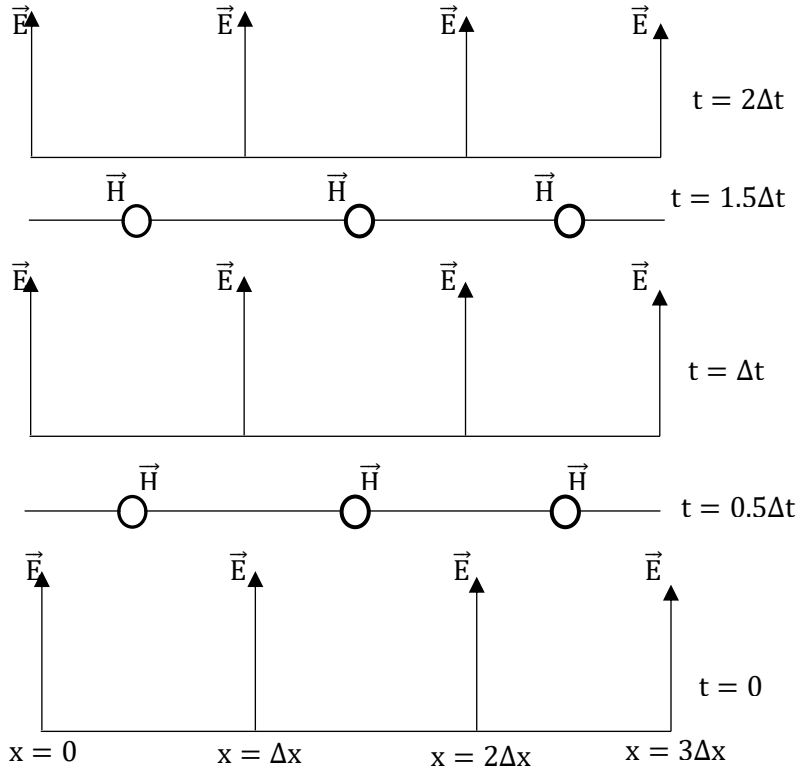

Figure 3.1: 1D scheme of FDTD method.

From the fig. 3.1, it is observed that the circulation of electric field $\vec{E}$ induces the magnetic field $\vec{H}$, likewise the circulation of magnetic field $\vec{H}$ induces electric field $\vec{E}$. So, at any point in space, the update value of electric field $\vec{E}$ in time, is dependent on the previous value of electric field and the numerical curl of the distribution of the magnetic field $\vec{H}$ in space. Again, at any point in space, the update value of magnetic field $\vec{H}$ in time, is dependent on the previous value of electric field and the numerical curl of the distribution of the electric field $\vec{E}$ in space. Thus, the electromagnetic propagation through the surface both in time domain and space domain. So, by calculating the update value of $\vec{E}$ field and $\vec{H}$ field at every point, the computational region can be obtained.

Using Yee's grid, the equations become

$$\frac{\partial E_x}{\partial t} = \frac{1}{\varepsilon}\frac{H_z(i,j) - H_z(i,j-1)}{\Delta y} \tag{3.17}$$

$$\frac{E_x^{n+1}\left(i+\frac{1}{2},j\right) - E_x^{n}\left(i+\frac{1}{2},j\right)}{\Delta t} = \frac{1}{\varepsilon}\frac{H_z^{n+\frac{1}{2}}\left(i+\frac{1}{2},j\right) - H_z^{n+\frac{1}{2}}\left(i+\frac{1}{2},j-\frac{1}{2}\right)}{\Delta y} \tag{3.18}$$

The electric field $\vec{E}$ and the magnetic field $\vec{H}$ are shifted in space by half a step and in time by one step using central difference approximation.

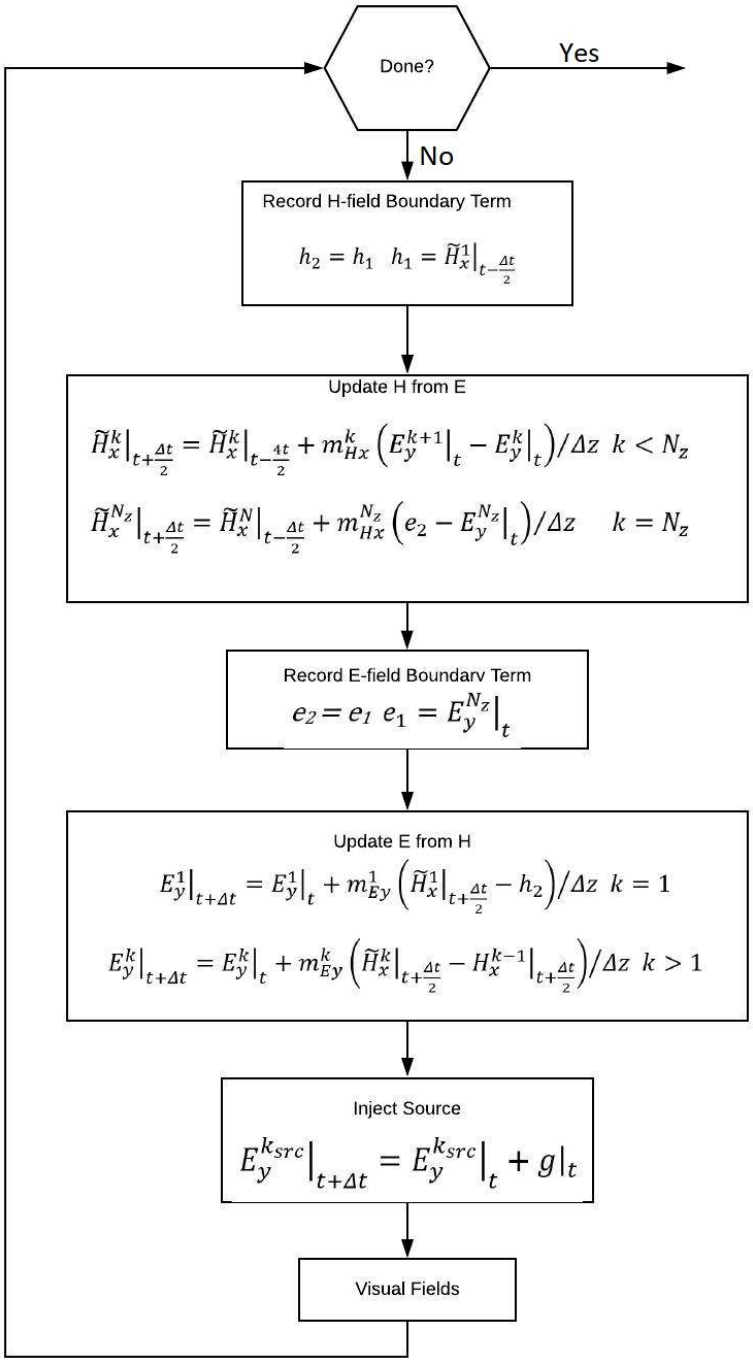

Figure 3.2: Flow Chart of FDTD Algorithm.

The algorithm helps to find out $\vec{E}$ field and $\vec{H}$ field using Yee's grid. Initially it assigns the number size of array and initialize value of $\vec{E}$ field and $\vec{H}$ field. Then from the curl equation and central difference approximation, the update equation of $\vec{E}$ field and $\vec{H}$

field are obtained. It calculates update value of $\vec{H}$ field from the $\vec{E}$ field. Keeping stored the value of $\vec{H}$ field then the update value of $\vec{E}$ field has been calculated. By Injecting source to the system, the electromagnetic field are visualized. Thus, the FDTD algorithm works to calculate electromagnetic field in the computational region.

3.3 Boundary Condition

In FDTD method, a space of theoretically infinite extent with a finite computational cell is simulated because the resources of computer is limited. In the case of a spatially limited structure, such as a waveguide, a resonator, etc., the problem does not exist where we need to model a region that "traps" the field within. However, we have to simulate open space regions in most of the issues. Because our simulation region must be limited in these cases, we need to create a boundary that absorbs outgoing signal to attenuate the propagation. For this, Berenger's perfectly matched layer (PML) have been proposed [15]. It's actually artificial boundary that prevent back reflection of outgoing signal. Using this boundary electromagnetic field is attenuated significantly and becomes zero at the end [16].

Chapter 4

4. Plasmonic Coupler and designing of coupler

4.1 Background

As we have seen that the interest in plasmonics have increased recently due to its important role in minimizing the space required to integrate multiple optoelectronic devices on a single chip. Due to this there's a huge increase in interest about plasmonic waveguides particularly formed by metal-dielectric-metal structures as this structure has the ability to tightly confine light in small region on sub wavelength scales. This confining of light is not possible with conventional dielectric waveguide due to diffraction limit [17]. So, this is a huge achievement for plasmonic waveguide. But there's a downside to this as well. In order to have good quality confinement the dielectric region of waveguide has to be made as smaller as possible. But due to this small size, it is seen that large propagation loss occurs in the waveguide [18]. That means the propagation loss hampers the advantage achieved from the confinement. So there has to be a tradeoff so that we can get maximum output from our waveguide. The best solution found for this scenario is to integrate a plasmonic waveguide and dielectric waveguide in the same system [19]. In order to achieve this combined waveguide system couplers idea was generated and that's why efficient coupler has a huge significance in modern plasmonics field.

4.2 Plasmon Coupling

Surface plasmons are a collective free electron density oscillation on the surface of metals in response to an external electric field. At close range this surface plasmons show a characteristic called plasmon coupling. A plasmon coupling is an event where the surface plasmons of adjacent nano particles interact with each other [20]. This coupled oscillation of electrons across the surface of two or more particles in close contact, causes the optical properties of the coupled particles to differ from that of an

individual particle in solution. The optical effects of plasmon coupling can be gigantic, depending on nanoparticle shape and size, interparticle spacing, number of plasmon coupled nanoparticles, light polarization and other factors. This effect can be used in different sectors to achieve different goals. In biological application it can be used to detect the presence of certain cell types and image them non-invasively. In plasmonics applications it can be used to connect dielectric waveguides with plasmonic waveguides.

4.3 Coupling Methods

The solution of reducing coupling loss is to integrate both waveguides using a coupler. Dielectric waveguides are used to connect plasmonic devices to the source so that the loss occurring due to metallic interaction are greatly diminished. To achieve that we need an efficient way of coupling the two waveguides. Several coupling methods have been suggested to increase the coupling efficiency as much as possible. Scientist named Wahsheh and Abushagur manifested an effective method for coupling light between plasmonic waveguides and dielectric waveguides. Dionne demonstrated subwavelength slot waveguides experimentally. Many distinctive plasmonic couplers have been proposed up to this point. Such as coupler with adiabatic and non-adiabatic tapered plasmonic coupler [27], nano-plasmonic air-slot coupler with fabrication processes [25], λ/4 coupler [28] etc. Saiful Islam et.al put forward a compact nano-plasmonic coupler of semi-elliptical form [24]. Waveguide having a tapered gap for adiabatic and nonadiabatic coupling was suggested by D.Pile. Rakibul Hasan et.al stated a study of semi-elliptical structured coupler having air gaps. A coupler optimized with multisection tapers was designed by G.Veronis [26]. New methods of coupling are being invented routinely to increase the efficiency as much as possible.

4.4 Design procedure of coupler

The coupler has to be designed in such a way that we can get maximum coupling efficiency from it. Higher efficiency means less propagation loss thus the advantages of plasmonics can be utilized in circuit designing. The first task is to choose a proper

material that will cause minimum loss in propagation. Then the structure has to be visualized. Then the most efficient value of parameters has to be calculated via trial and error by varying some parameters which would be discussed in the later sections.

4.5 Choice of Materials

4.5.1 Parameters for Choosing Materials

The choice of materials is done in such a way that the amount of loss in plasmonic waveguides can be reduced as much as possible. The reason behind one of the most significant loss in these cases are the transitions of electrons among the energy bands at optical frequencies. The reason for this is that the valence band electrons jump to conduction band due to the energy absorption from photons which results in transmission loss. So, in order to minimize these losses, we have to use materials with higher bandgap. Also, dispersive properties of materials should be considered as well.

4.5.2 Band Gap

A band gap is a range of energy in solid where there will be no electron state. In case of band structure of solids, the band gap means the energy difference in eV between top of the valence band and the bottom of the conduction band in semiconductor. So, in a way it's the energy required to move a valence electron to conduction band thus converting to conduction electron, which is free to move within the crystal and serve as electric current. The band gap is therefore a significant factor that determines a solid's electrical conductivity. Substances with wide band gaps are usually insulators, those with smaller band gaps are semiconductors, and conductors have either very small band gaps or none because the bands of valence and conduction overlap [21]. Data from Kittel, C., Introduction to Solid State Physics, 6th Ed., New York: John Wiley, 1986, p 185 shows some of the materials bandgap in eV which is tabulated in table 4.1 below:

Table 4.1: Band Gap Values for Different Materials

Material	Energy gap (eV)	
	0K	300K
Si	1.17	1.11
Ge	0.74	0.66
InSb	0.23	0.17
InAs	0.43	0.36
InP	1.42	1.27
GaAs	1.52	1.43
GaSb	0.81	0.68
ZnS	3.91	3.6

4.5.3 Dispersion property

Dispersion means to form a homogenous solution of any nanoparticles. It is a composition of at least 2 materials and this composition has at least 2 separate phases, one of which is the continuous phase and the other one is dispersed phase. Dispersion degree strongly influences the rheological properties of suspension-containing nanosized particles and, as a result, the consistency of the deposited film. In fact, their implementations will be strictly limited if the weak dispersion can not be effectively resolved. So, while choosing the material good dispersion quality materials has to be chosen.

4.5.4 Final selection of materials

As seen from the above-mentioned table, the bandgap of GaAs varies between 1.43 ev to 1.52 ev, which is quite large thus helps in neglecting inter-band transmission losses. Also, GaAs can be constructed into very thin layers which can store huge energy within smaller devices. Considering the great dispersive properties of silver, it has been used as the metal and air has been used as the dielectric of the plasmonic waveguide.

4.6 coupling structure formation

4.6.1 Waveguide structure

A waveguide is a structure that guides waves, such as electromagnetic waves or sound, with minimal loss of energy by restricting the transmission of energy to one direction. It is a special transmission line type that is a hollow metal pipe. A waveguide does not have a center conductor, as opposed to a transmission line. These are easy to produce and can handle very high power. There are five types of waveguides.

- Rectangular waveguide
- Circular waveguide
- Elliptical waveguide
- Single-ridged waveguide
- Double-ridged waveguide

Some sample figures of the waveguides are presented in fig 4.1:

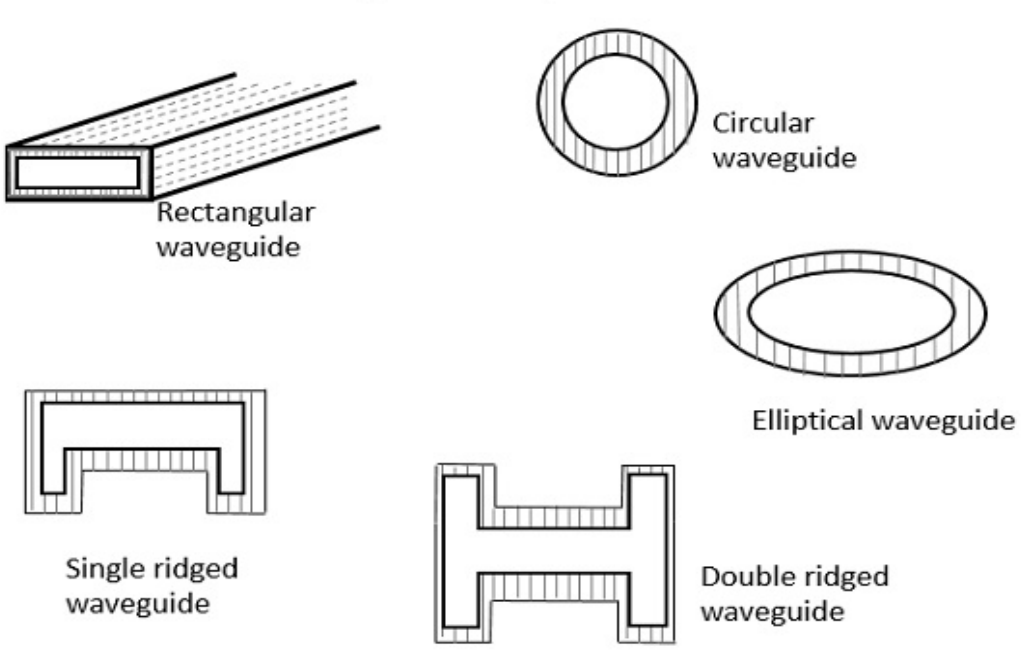

Figure 4.1: Different waveguide structures [35].

Different waveguide structures have different advantages and disadvantages. Considering the structure which will be of most benefit to us we selected rectangular waveguide. Rectangular waveguides are one of the earliest type of waveguides discovered. They are used in many applications. A rectangular waveguide supports TM and TE modes but not TEM waves because unique voltage can't be defined because in a rectangular waveguide there is only one conductor. Under a certain frequency, a rectangular waveguide can not propagate, this frequency is called the cut-off frequency.

4.6.2 Overviewing few coupler structures

As the advantages of plasmonics were imminent and the world saw its huge potential, the use of plasmonics greatly increased. With the increased usage of plasmonics the need to remove the propagation loss arose which was meant to be solved by coupler which will couple dielectric waveguide and plasmonic waveguide. That is Dielectric waveguide for propagating long distances and plasmonic waveguide for sub-wavelength scale transmission, while coupler comes in between them.

Seeing the huge need of coupler in modern plasmonics different researchers came up with different ideas of coupler which consisted of different shapes, materials and sizes. For our designing purpose we overviewed few of the couplers previously designed by different researchers to get a vivid idea about how these structures are now a days and which can be used to improve the quality even further.

One of the basic couplers we found was the Cuprous oxide-based ultra-compact nano-plasmonic coupler designed by Md. Ghulam Saber & Rakibul Hasan Sagor [22]. The Cu_2O layer width was taken as 300 nm and the air layer width was taken as 60 nm in the MIM waveguide. This coupler yields 56 percent coupling efficiency at a wavelength of 1,550 nm. The structure of the coupler is shown in fig. 4.2.

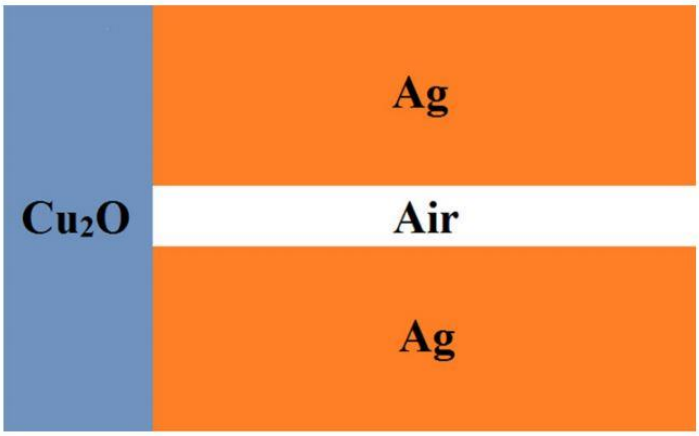

Figure 4.2:Cuprous oxide-based ultra-compact nanoplasmonic coupler [22].

Another basic structure is the Gallium Lanthanum Sulfide based Nanoplasmonic Coupler designed by Rakibul Hasan Sagor, Md. Ashraful Hoque and Md. Ghulam Saber [23]. The length of the GLS layer is 300 nm for this coupler and the width of the air layer is 60 nm in the MDM waveguide. For this reason, a coupling efficiency of 67% was achieved at the optical wavelength of communication. The structure is shown in fig 4.3.

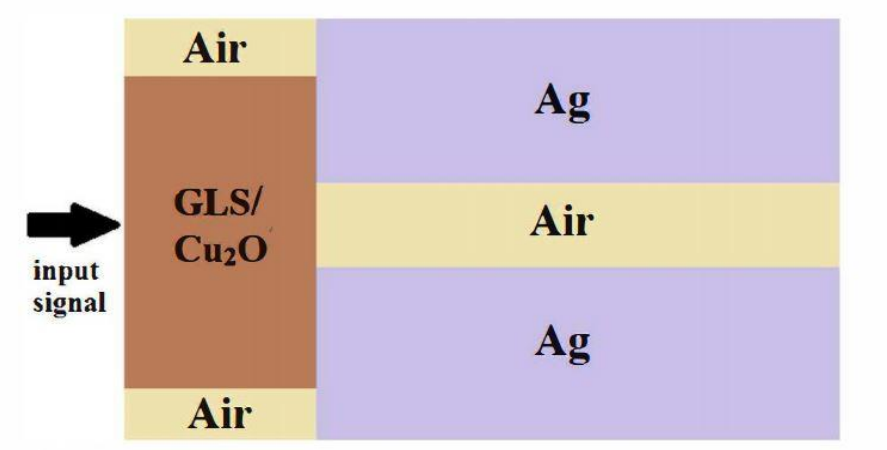

Figure 4.3: Gallium Lanthanum Sulfide based Nanoplasmonic Coupler [23].

We also found a few couplers which used complex shapes inserted in them like semi-elliptical, elliptical or circular etc. These complex structures gave a higher efficiency than the basic ones. One of these structures are A Semi-Elliptical Ultra-Compact Nano-plasmonic Coupler by Saiful Islam Sumon, Mahir Tazwar, Rakibul Hasan Sagor and Sakib Mahtab Khandaker [24]. Here Dielectric (silicon) length has been chosen as 300 nm.The height is taken as 300 nm. The coupler is a semi-elliptical structure with a semi-minor length of axis identified by ‘a’ and semi-major axis defined by ‘b’. The parameter

'W_p' determines the length of the plasmonic waveguide. This proposed coupler yields at optical communication wavelength a coupling efficiency of 78%. The coupler is shown in fig. 4.4.

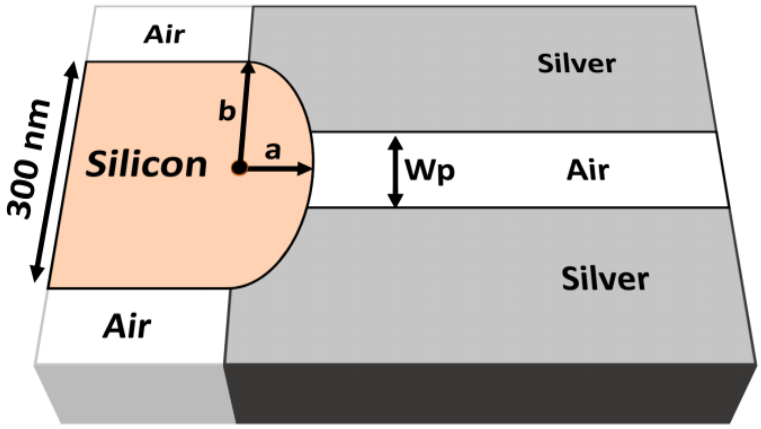

Figure 4.4: A Semi-Elliptical Ultra-Compact Nano-plasmonic Coupler [24].

Then we found a coupler which introduces a new parameter, an air slot in the dielctric waveguide. This air slot feature was very new and there was not much work done using these features. Researchers named R. A. Wahsheh and M. A. Abushagur first thought of this idea of an air slot based coupler and designed one basic structure with it [25]. The height of the silicon and plasmonic waveguides is 250 nm. The dielectric air-slot waveguide is expected to increase the coupling efficiency at the interface with the plasmonic waveguide because the field within the dielectric air-slot waveguide matches that in the plasmonic air-slot waveguide. The researchers found that the air slot did increase the efficiency of a normal coupler by around 20%. The following structure by Rami achieved a coupling efficiency of around 63%.

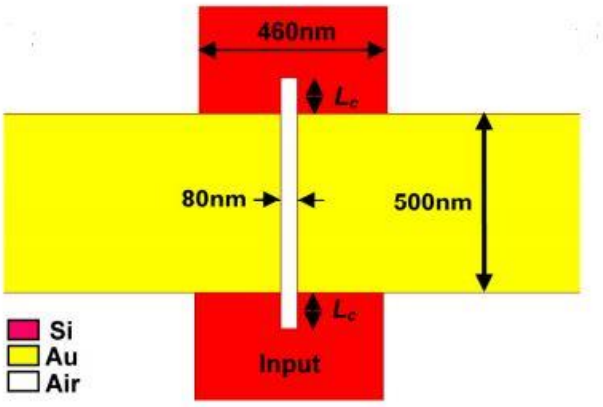

Figure 4.5: An air-slot coupler between dielectric and plasmonic waveguides [25].

4.6.3 Final structure

Reviewing the advantages of air slot in couplers as found by R. A. Wahsheh and M. A. Abushagur [25], we thought of implementing a new coupler with the feature of air slot in it. As the coupler proposed by R. A. Wahsheh and M. A. Abushagur with air slot, had a poor efficiency, a newer coupler with new structure might help the efficiency. So we designed a new coupler which has a three-dimensional rectangular structure with Galium Arsenide (GaAs) considered as the dielectric waveguide. There's an air slot added inside the dielectric waveguide. For MDM waveguide as well, a three-dimensional rectangular structure is chosen with metal selected as silver and with air as the dielectric. An illustrative view of the structure is shown in fig. 4.6. The width of GaAs is taken as 400 nm and the length of the metal is kept at 100 nm. The air gap width of the MDM waveguide is denoted as parameter 'a', the air-slot distance is denoted as parameter 'b' and the coupler height is denoted as 'h'.

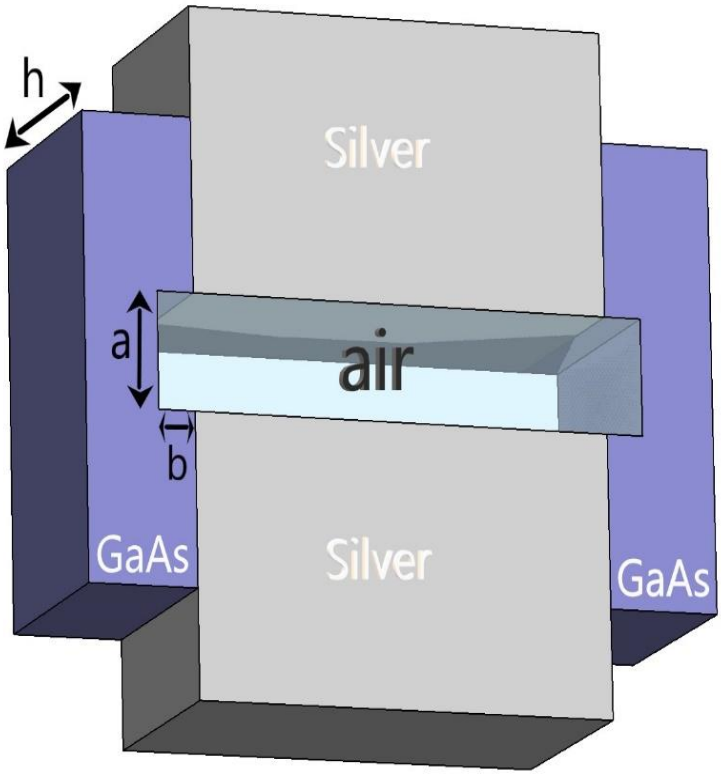

Figure 4.6:3D view of the proposed coupling structure.

Chapter 5

5. Performance Analysis of Plasmonic Coupler

5.1 Efficiency Analysis

To determine the efficiency of designed coupler, we have considered some parameters regarding the structure. The parameters value should be assigned in such a way that we can get maximum efficiency of our coupler. Basically, we are working with rectangular shaped coupler that has metal-dielectric-metal waveguide, dielectric waveguide and air slot that is inserted into dielectric material. The interface of metallic region and dielectric region in the MDM waveguides is an important part in the analysis process that contributes to increase the performance of coupler. So, air is taken into account as dielectric material to create interface in MDM waveguide and also to couple the dielectric waveguide of the coupler. Because of that, the parameters which we have considered for our analysis process to compute coupling efficiency are given as followed:

1. Air Gap of MDM Waveguide, ‘a’.
2. Air Slot inserted into Dielectric Waveguide, ‘b’.
3. Height of the coupler, ‘h’.

5.1.1 The effect of Air Gap variation of MDM Waveguide

Air Gap implies an impact on plasmonic coupler which we have observed from the simulation results. Air Gap has been varied manually and data has been taken from the result tool in CST software. the efficiency of coupler is changing with the variation of Air Gap. The electromagnetic field (EM) is also changing because of Air Gap. Among the parameters, firstly Air Gap has been varied to calculate coupling efficiency keeping other parameters fixed.

The coupling efficiency of the nano-plasmonic coupler using Galium Arsenide (GaAs) as a function of wavelength has been determined with variation of air gap from ‘a’=10

nm to ‘a’=120 nm. The air gaps are incremented with a value of 10 nm. The coupling efficiency and the structure at 60 nm, 100 nm and 120 nm of air gap has been presented below.

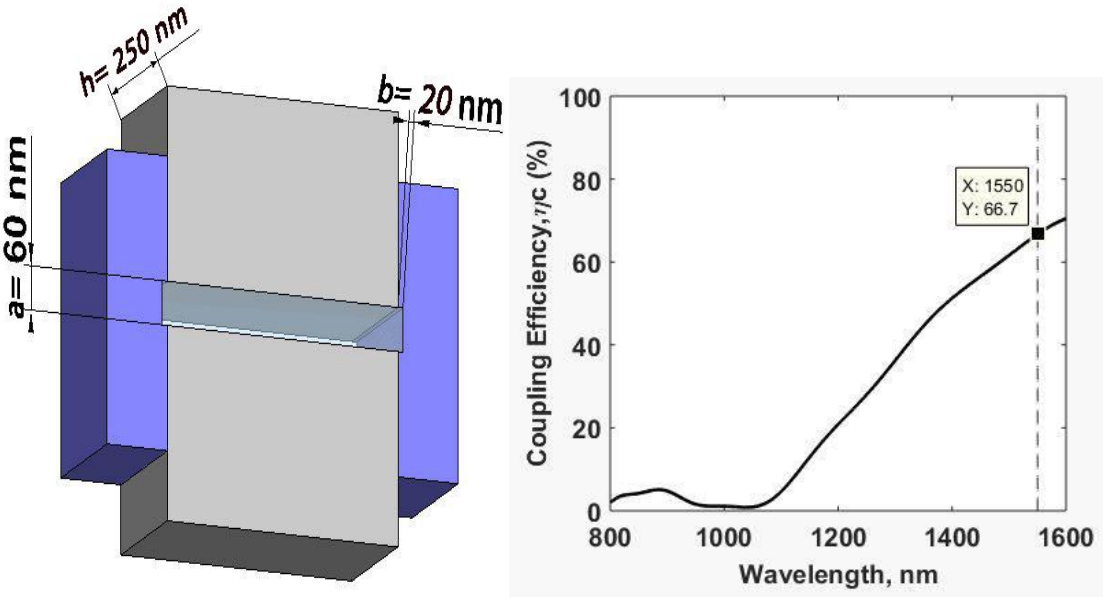

(a) Proposed 3D structure (b) Coupling efficiency vs Wavelength

Figure 5.1: 3D Coupling structure and efficiency at a=60 nm, b=20 nm & h=250 nm

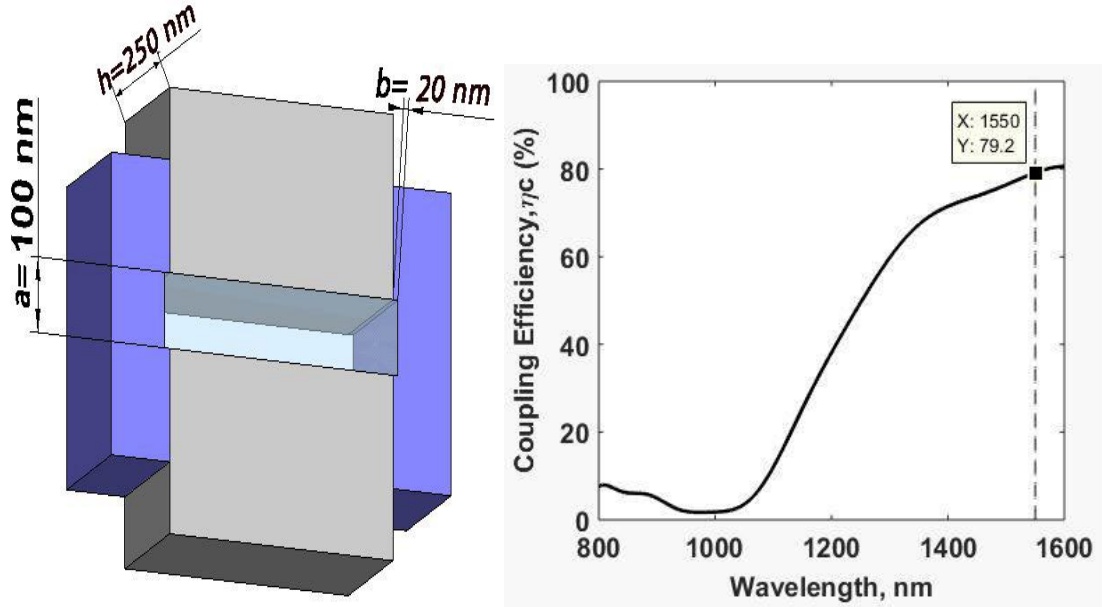

(a) Proposed 3D structure (b) Coupling efficiency vs Wavelength

Figure 5.2: 3D Coupling structure and efficiency at a=100 nm, b=20 nm & h=250 nm

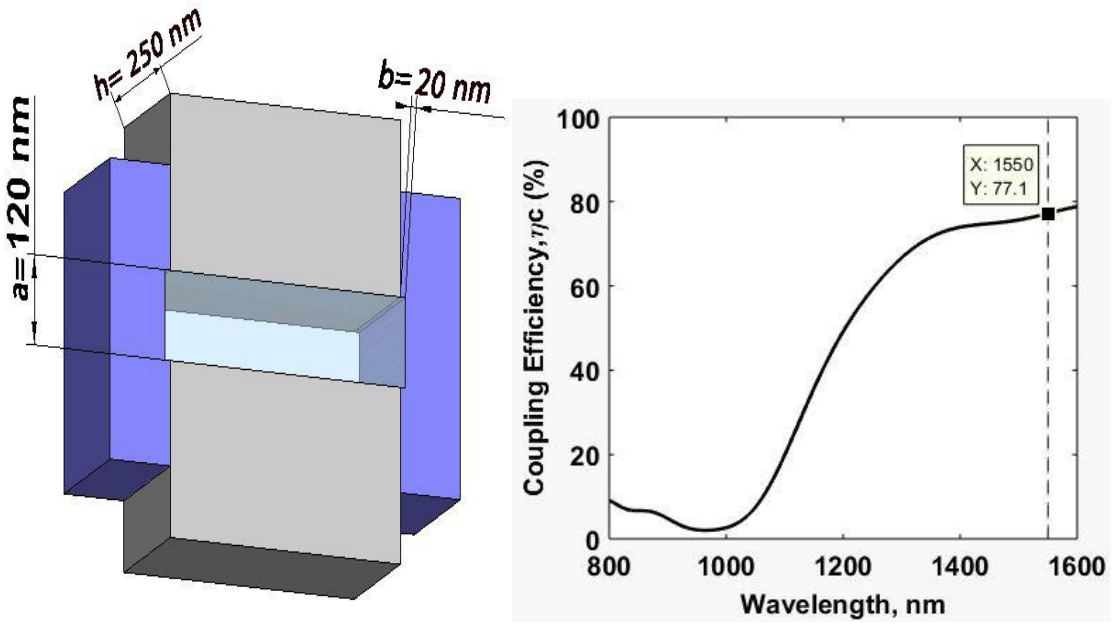

(a) Proposed 3D structure (b) Coupling efficiency vs Wavelength

Figure 5.3: 3D Coupling structure and efficiency at a=120 nm, b=20 nm & h=250 nm

After all the values for 'a'=10 nm to 'a'=120 nm is determined, all the wavelengths vs efficiency is plotted in the same figure in fig. 5.4, which is shown below:

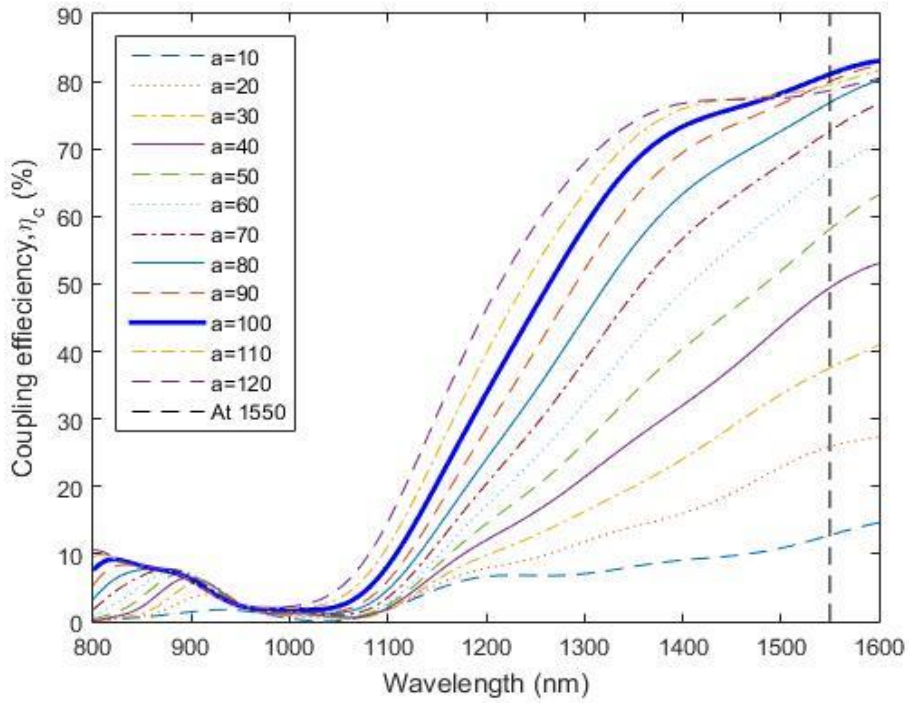

Figure 5.4: Coupling Efficiency vs Wavelength due to variation of airgap length.

Then at optical communication wavelength (1550 nm) the efficiencies are measured and plotted against different values for ‘a’ in fig 5.5, which is shown below:

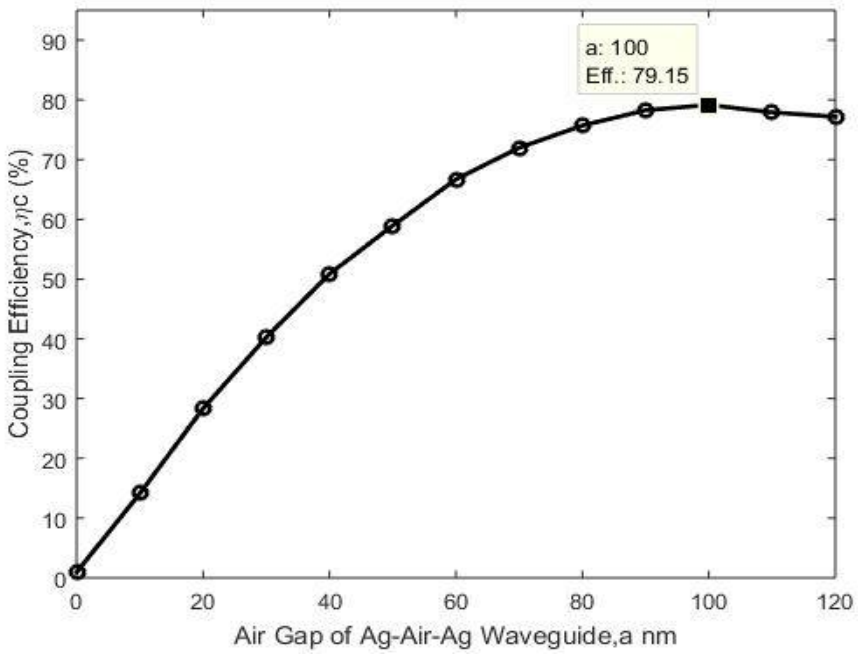

Figure 5.5: Coupling Efficiency vs Air Gap of MDM waveguide.

From the figure, it can be observed that the coupling efficiency keeps on increasing as we increase the air gap of dielectric region of MDM waveguide up to ‘a’=100 nm, after that it decreases. We have calculated performance parameters at optical communication wavelength (1550 nm) because our designed coupler is mostly proposed for 1550 nm wavelength. At 100 nm, the maximum efficiency (79.15%) has been found as shown in figure 5.5.

5.1.2 The effect of Air Slot of Dielectric Waveguide

As mentioned, the coupling efficiency is dependent on air Slot as well. So, with the variation of Air Slot, the performance parameters like coupling efficiency, transmittance coefficient and reflectance coefficient are also changing. To obtain more efficiency of the coupler, keeping ‘a’=100 nm, air slot has been varied from ‘b’=0 nm to ‘b’=50 nm with step size 5 nm. Among these air slot values, for 5 nm, 15 nm and 30 nm the coupling structure and corresponding efficiency is presented below:

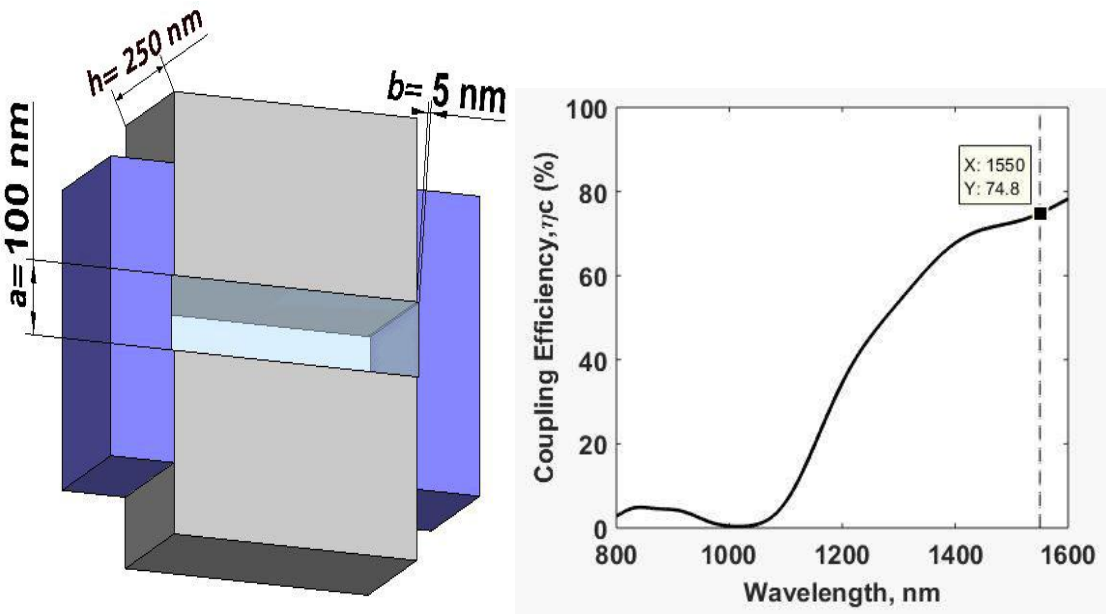

(a) Proposed 3D structure (b) Coupling efficiency vs Wavelength

Figure 5.6: 3D Coupling structure and efficiency at a=100 nm, b=5 nm & h=250 nm.

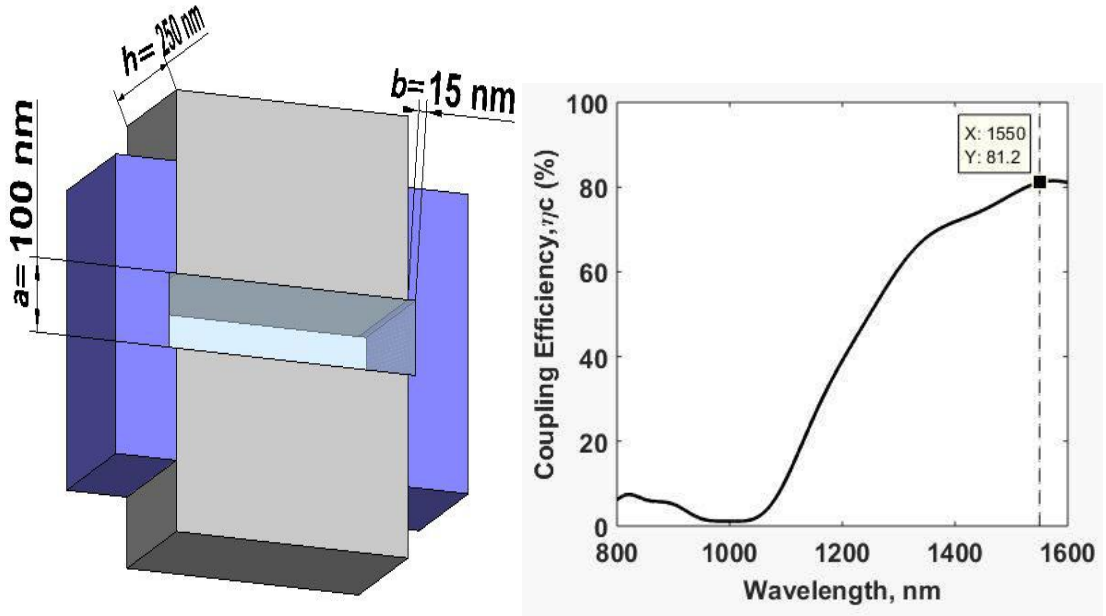

(a) Proposed 3D structure (b) Coupling efficiency vs Wavelength

Figure 5.7:3D Coupling structure and efficiency at a=100 nm,b=15 nm & h=250 nm.

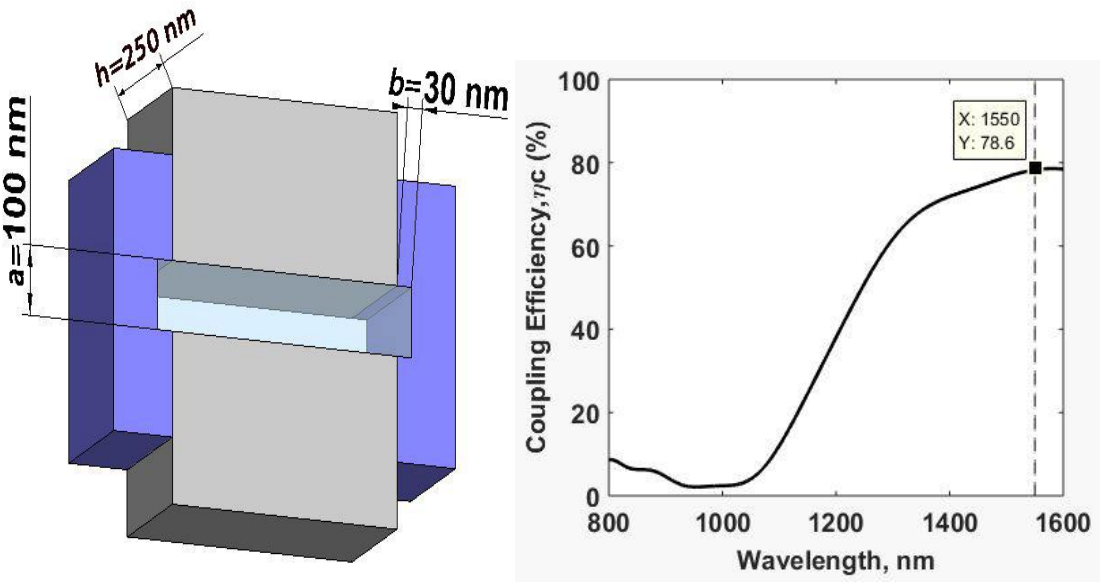

(a) Proposed 3D structure (b) Coupling efficiency vs Wavelength

Figure 5.8: 3D Coupling structure and efficiency at a=100 nm,b=30 nm & h=250 nm.

After all the values for 'b'=5 nm to 'b'=30 nm are determined, all the wavelengths vs efficiency are plotted in the same figure in fig 5.9, which is shown below:

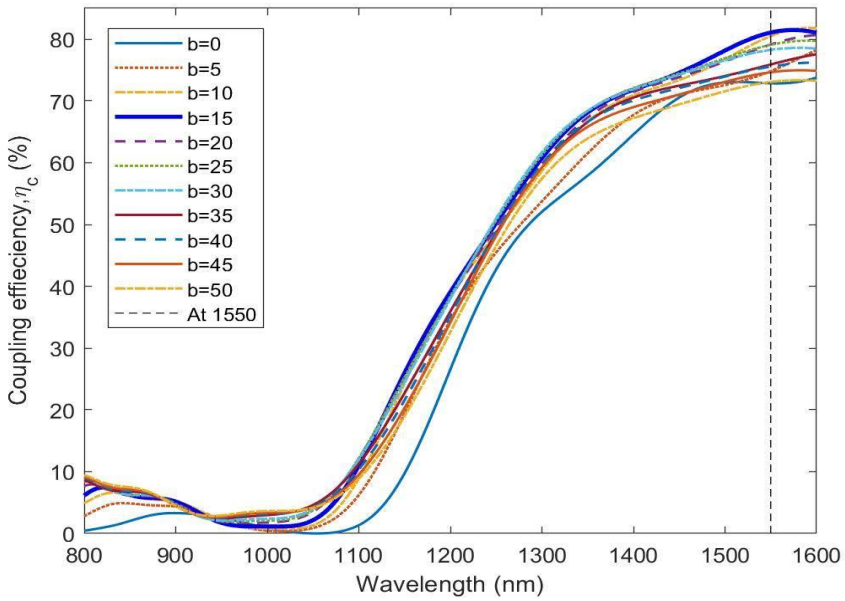

Figure 5.9: Coupling Efficiency vs Wavelength due to variation of airslot inserted.

The dependency of coupling efficiency on air slot at communication wavelength (1550 nm) has been calculated and at 'b'=15 nm the maximum efficiency (81.07%) is found which is presented in Fig.5.10.

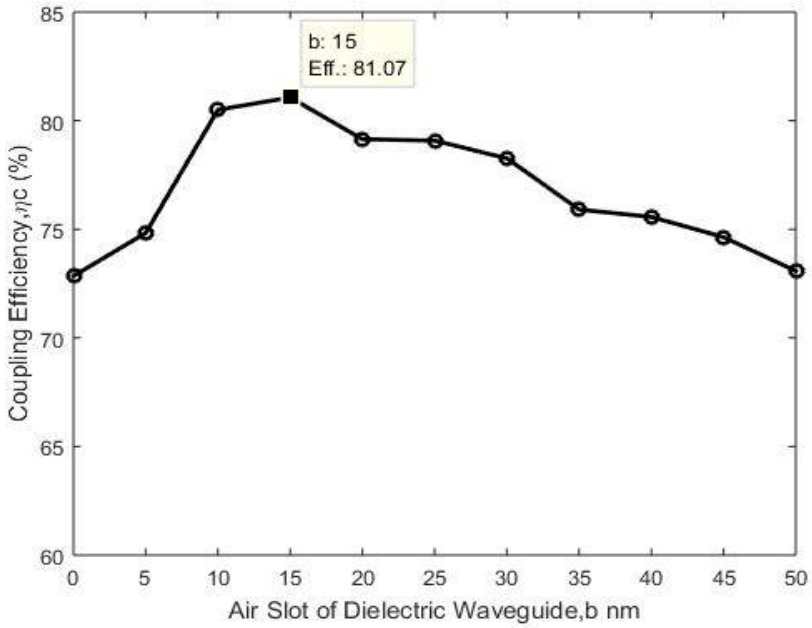

Figure 5.10: Coupling Efficiency vs Air Slot in Dieletric Waveguide.

5.1.3 The effect of Coupler Height Variation

To further optimize the efficiency value for our proposed coupler the variation of height from 'h'=220 nm to 'h'=265 nm is made. Among these values, at 235 nm, 250 nm and 265 nm the coupling structure and corresponding efficiency is presented below:

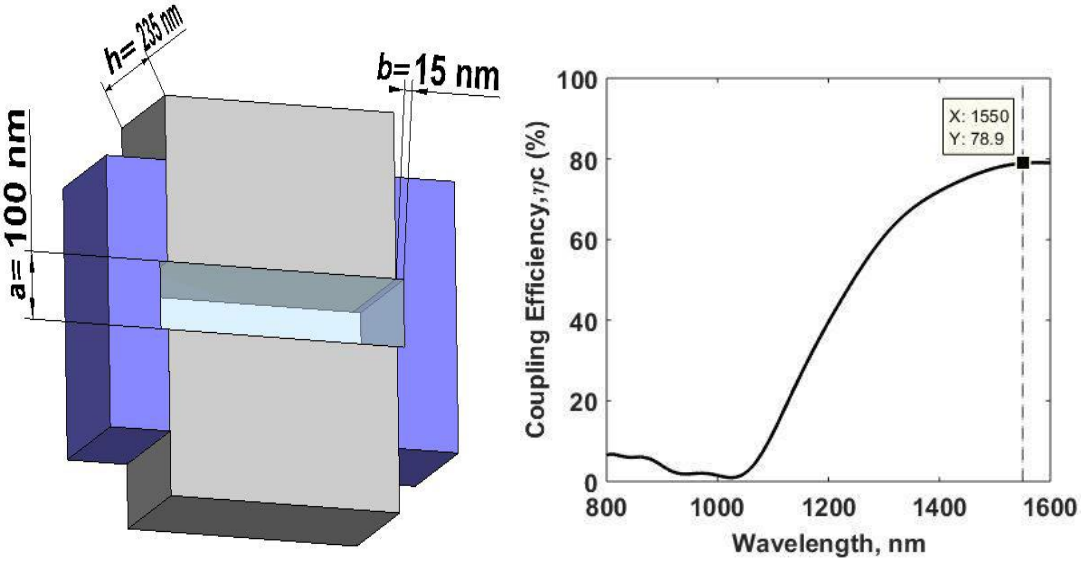

(a) Proposed 3D structure (b) Coupling efficiency vs Wavelength

Figure 5.11: 3D Coupling structure and efficiency at a=100 nm, b=15 nm & h=235 nm

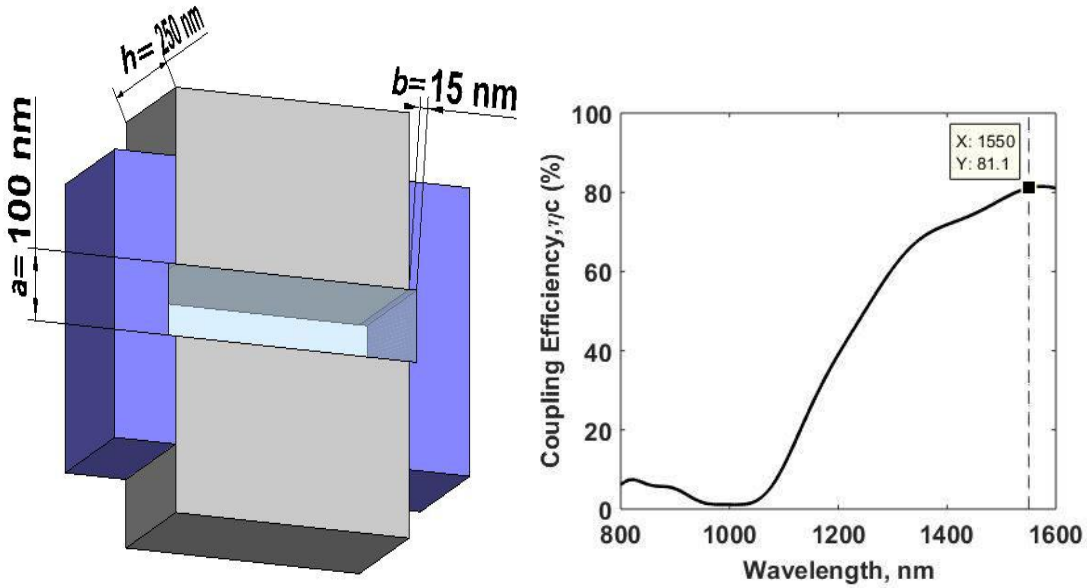

(a) Proposed 3D structure (b) Coupling efficiency vs Wavelength

Figure 5.12*:* 3D Coupling structure and efficiency at a=100 nm, b=15 nm & h=250 nm.

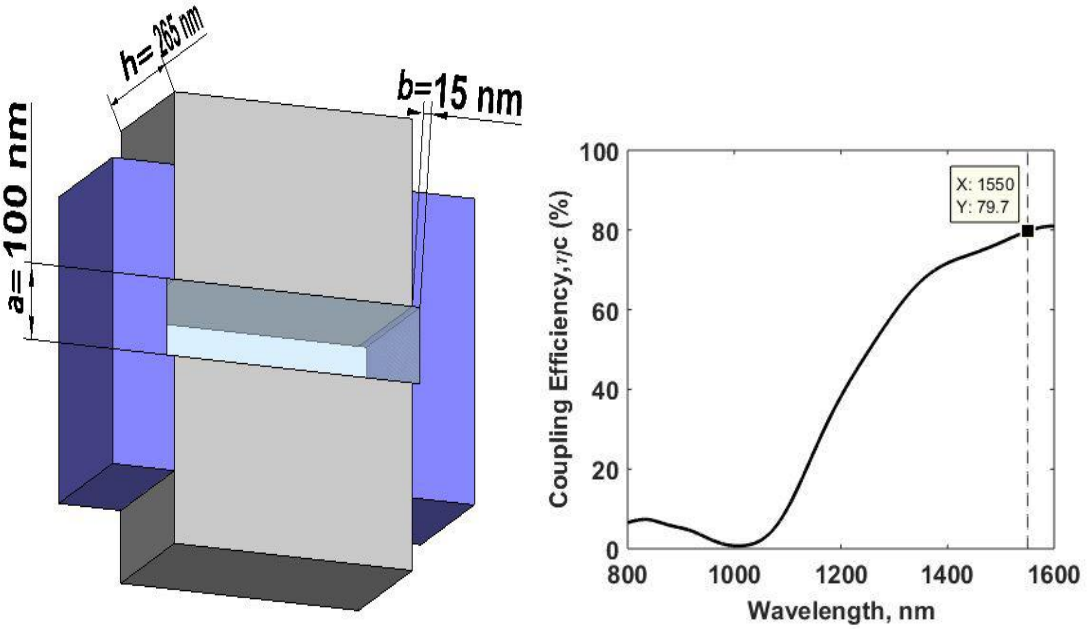

(a) Proposed 3D structure (b) Coupling efficiency vs Wavelength

Figure 5.13: 3D Coupling structure and efficiency at a=100 nm, b=15 nm & h=265 nm.

After all the values for h=220 nm to h=265 nm are determined, all the wavelengths vs efficiency are plotted in the same figure in fig. 5.14, which is shown below:

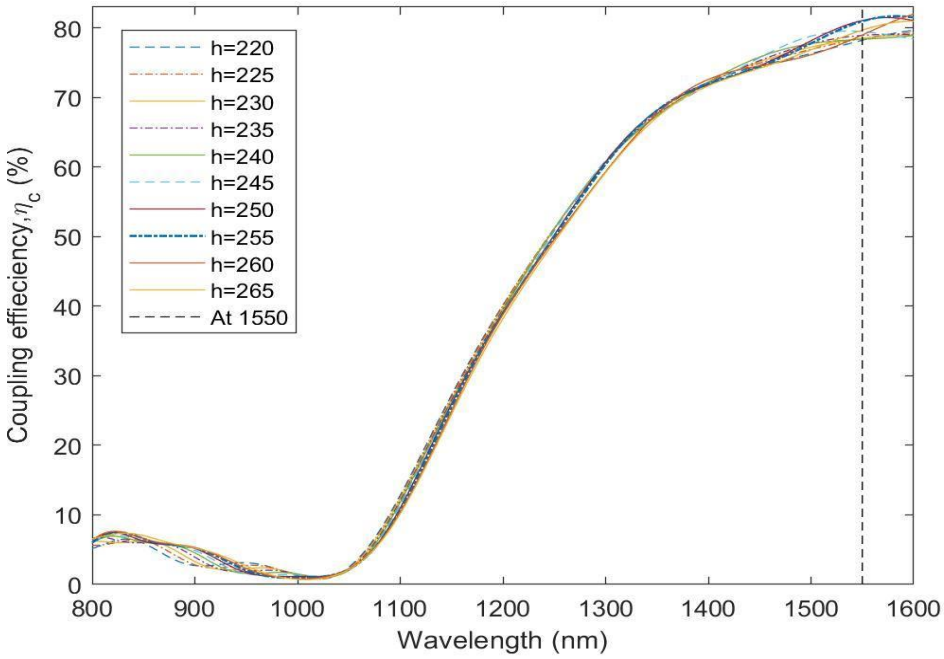

Figure 5.14: Coupling Efficiency vs Wavelength due to variation of height.

From the figure, it is observed that the value of coupling efficiency remained more or less constant up to 'h'=240 nm, then it started increasing and at 250 nm maximum coupling efficiency (81.07%) is obtained that is provided in Fig. 5.15.

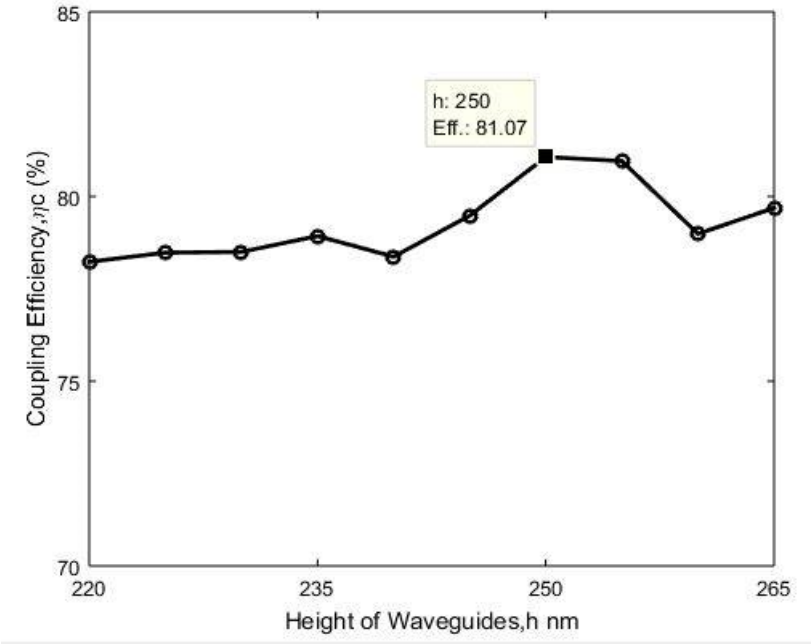

Figure 5.15: Coupling Efficiency vs Height of Waveguides

In Table 5.1 maximum efficiency at any wavelength (800 nm -1600 nm) due to variation of air gap, air slot and height of waveguide has been tabulated.

Table 5.1: Maximum efficiency at any wavelength

Parameter	Maximum efficiency at 800-1600 nm wavelength		
	Efficiency (%)	Optimal value (nm)	Wavelength (nm)
Air gap, ‘a’	83.01	100	1600
Air slot, ‘b’	81.94	10	1590
Height, ‘h’	81.99	260	1600

In table 5.2 the efficiency of coupler at optical communication wavelength (1550 nm) has been tabulated due to variation in parameters. This tables show overview about overall coupling efficiency for our Galium Arsenide (GaAs) based coupler.

Table 5.2: Maximum efficiency at 1500 nm wavelength

Parameter	Maximum efficiency at 1500 nm wavelength	
	Efficiency (%)	Optimal value (nm)
Air gap, ‘a’	79.15	100
Air slot, ‘b’	81.07	15
Height, ‘h’	81.07	250

5.2 Normalized Power Performance

5.2.1 Normalized Power

Normalized Power is a power averaging method, measured in watts, used to compensate for changes in conditions for a more accurate depiction of power expenditure. It is quite easy to understand and quantify to take Average Power by simply averaging the highs and lows of an effort over a given period. But its use is somewhat constrained. But the normalized power is difficult to understand but it might become helpful regarding some parameter’s analysis.

5.2.2 Analysis of Performance Parameters

At optical communication wavelength, our proposed coupler with optimal dimension

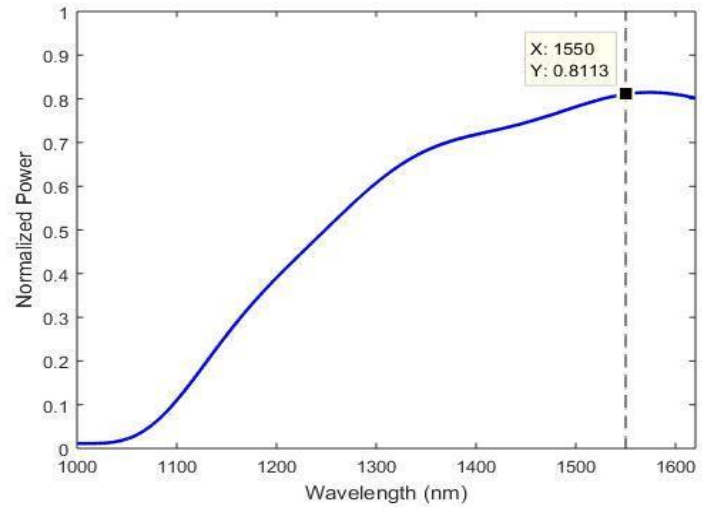

(a)Transmittance

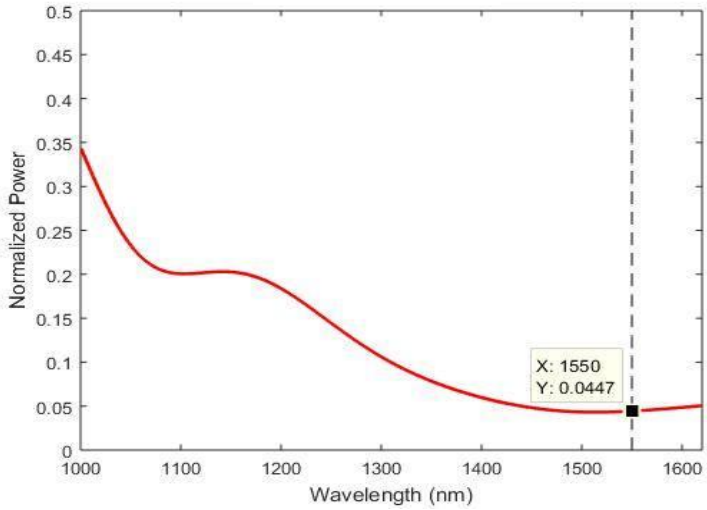

(b) Reflectance

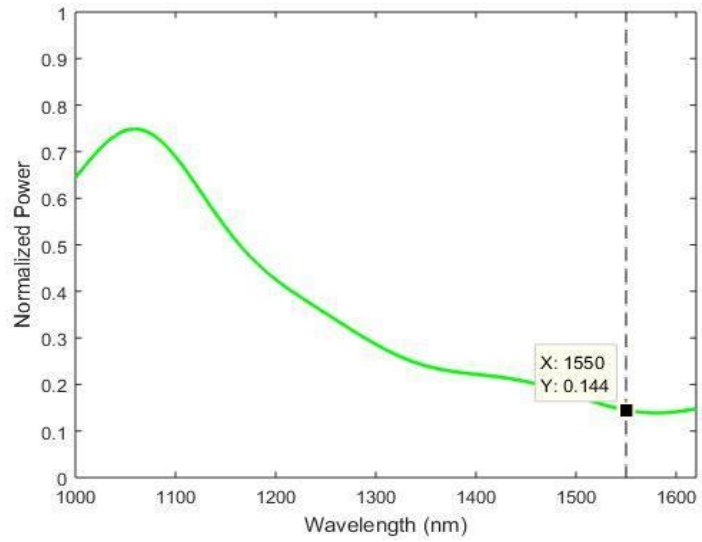

(c) Absorbance

Figure 5.16: Simulation results of different performance parameters for the coupler with wavelength.

(‘a’=100 nm, ‘b’=15 nm and ‘h’=250 nm) shows maximum efficiency of 81.07%. Keeping same optimal dimensions for calculating normalized power to verify the obtained results of our coupler. Normalized power depending on wavelength has been given in Fig. 5.16.

Different parameters such as normalized value of Transmittance, Reflectance and Absorbance has been tabulated in Table 5.3. From Table 5.3, it is observed that the summation of normalized power is 1, which satisfies the condition of total power.

Table 5.3: Performance parameters at 1550 nm

Performance parameters	Normalized value
Transmittance	0.811
Reflectance	0.045
Absorbance	0.144

5.3 Electric Field Distribution

5.3.1 Analysis of Electric Field Distribution

The electric field distribution at the surface of Galium Arsenide (GaAs) based coupling structure at optical communication wavelength (1550 nm) has been presented in Fig. 5.17. From the color map of the figure, it can be visualized that the field intensity is higher in the dielectric region comparing to the metallic layer of plasmonic waveguide because propagation loss is higher in metallic layer resulting in reduction of propagation length. Thus, sharp attenuation is obtained there. Propagation distance can be raised significantly due to coupling of both dielectric and plasmonic waveguides.

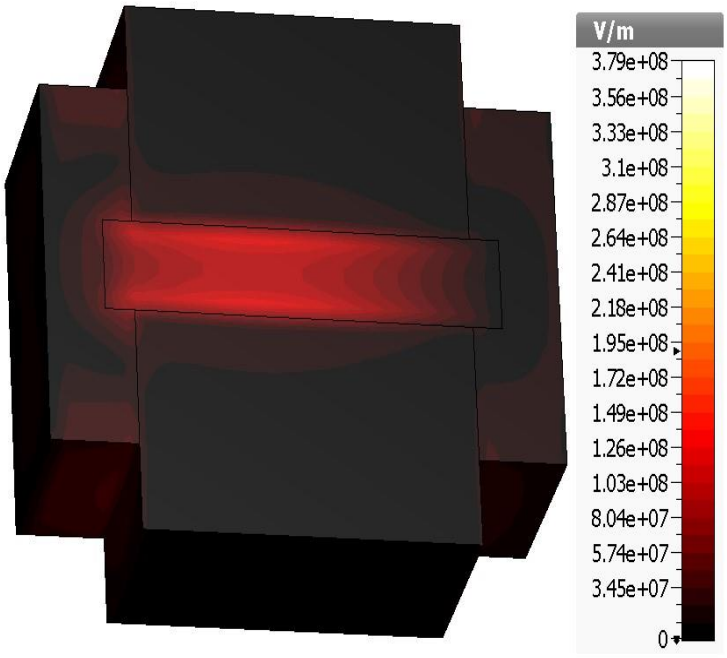

Figure 5.17: Electric field distribution at communication wavelength (1550 nm).

5.3.2 Cross Sectional view of Electric Field distribution

For visualizing the electric field more clearly, cross sectional view of electric field intensity has been taken twice, once at 50 nm and another at 350 nm away from the starting of plasmonic waveguide which is provided in Fig. 5.18.

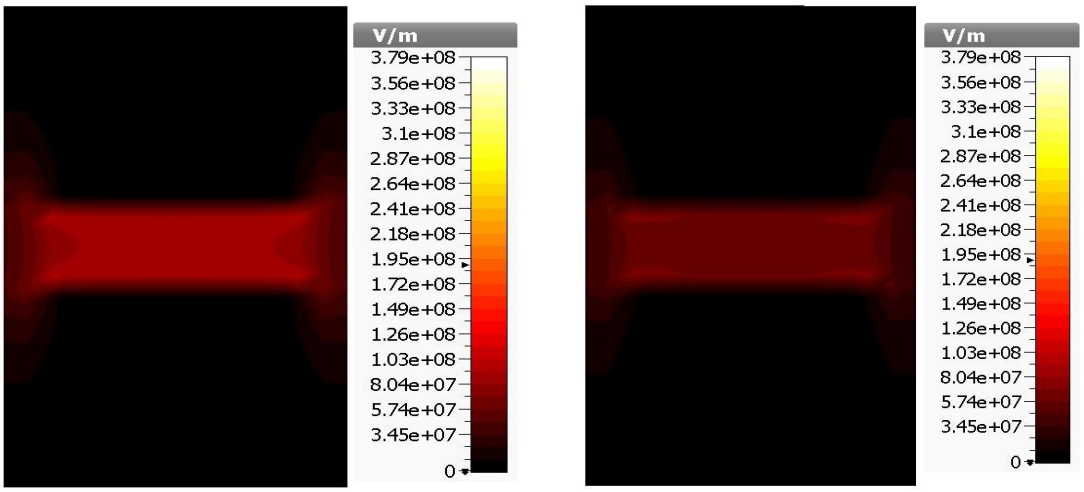

(a) 2D view of the electric field distribution at 50 nm

(b) 2D view of the electric field distribution at 350 nm

Figure 5.18: Cross sectional view of the electric field distribution at particular distances from the interface of dielectric and MDM waveguides.

From the figures, we can see that as the distance of MDM is increasing the corresponding electric field intensity is decreasing. So electric field intensity is reciprocal to the length of metal-dielectric-metal waveguide.

5.4 Limitations

While simulating the results we stumbled across a few events where our simulations were giving results which were not expected. For instance, for our designing, we considered that the airgap was at the center of the plasmonic waveguide. But if we move the airgap further above or below the center of the plasmonic waveguide then it shows abnormality in its behavior. The efficiency value decreases abruptly and goes below 5% which is completely unexpected. So, to get the desired efficiency we must have to keep the air gap at the center. A sample figure is shown when the airgap is taken 125 nm from the top of the plasmonic waveguide.

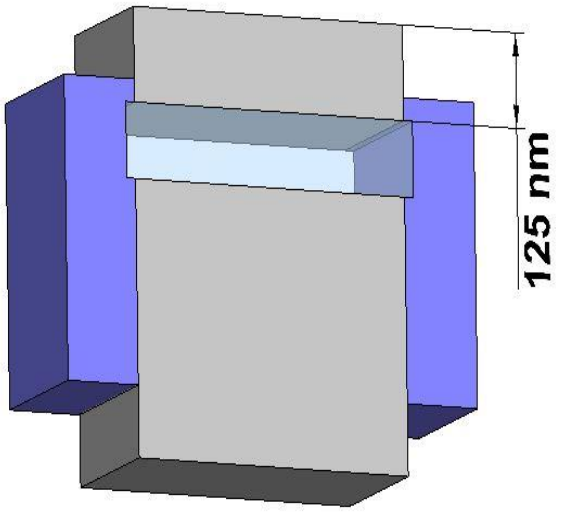

Figure 5.19: coupler structure when the airgap is at 125 nm from the top of MDM waveguide.

Fig. 5.20 shows the efficiency vs wavelength at that structure. This graph shows that the coupling efficiency is very low at any wavelength. At optical communication wavelength of 1550 nm it is less than 3.5% which is unexpected.

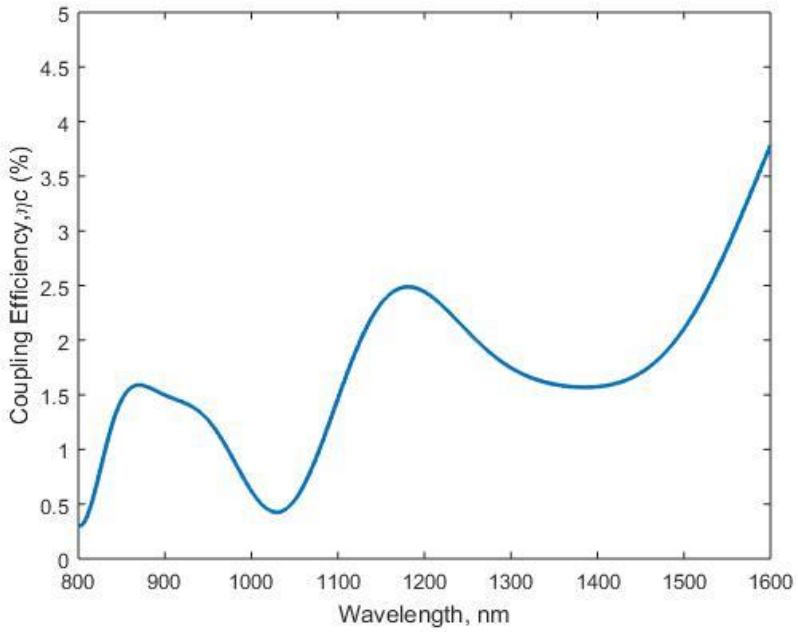

Figure 5.20 : Coupling efficiency vs wavelength at 125 nm from the top of MDM waveguide

Another anomaly we faced was the position of the port. Normally we placed the input port at the starting of the interface of the dielectric and output port at the end of dielectric waveguide. But if this position is changed it drastically changes the outcome. Like, if the output port is moved before the 2nd interface of plasmonic and dielectric waveguide the efficiency becomes really unpredictable, sometimes it crosses the value 100% and gives abnormal outcome. So, for our simulations the port was always taken at the start and end of dielectric waveguide. A sample figure of the normal situation of port and when the port was at 50 nm from the 2nd interface of the dielectric and plasmonic waveguide is shown in fig. 5.21.

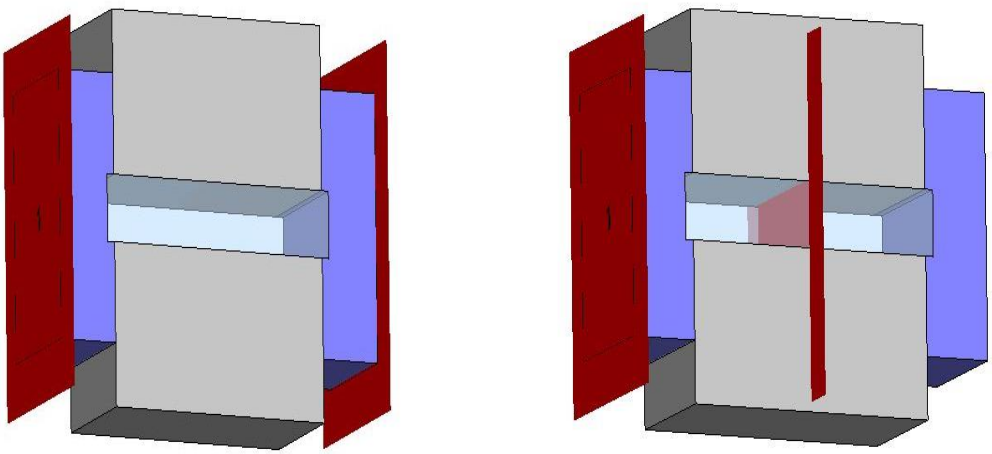

(a) Port position at start & end (b) port position at 50 nm from 2nd interface

Figure 5.21: Coupler structure at different position of ports.

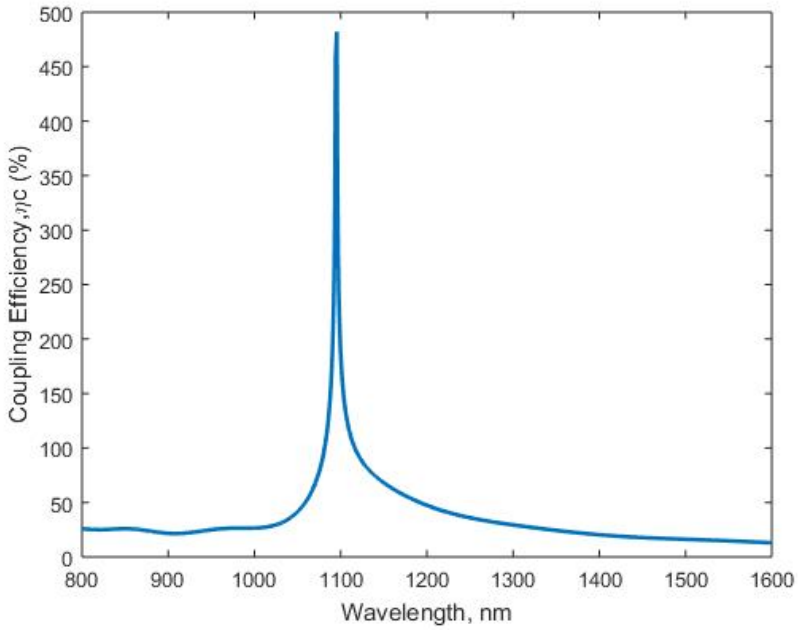

Figure 5.22 : Coupling efficiency vs wavelength when port is at 50 nm left from the 2nd interface

The coupling efficiency vs wavelength curve when the port was at 50 nm from the 2nd interface of the dielectric and plasmonic waveguide is shown in fig. 5.22 which shows us that the efficiency value is really abnormal and it reaches a maximum value of 460% approx. Also, the slope in which the efficiency value is decreasing is very non-practical which is unexpected.

Chapter 6

6. Conclusion and Future work

6.1 Conclusion

Contemplating the prominence of efficient plasmonic couplers to integrate dielectric and plasmonic waveguides in the present trend of miniaturization, a novel nanoplasmonic coupler deploying GaAs has been proposed. The suggested coupling structure has been finalized by optimizing different parameters like air slot length, air gap width of MDM plasmonic waveguide, and height. The most optimized structure leads to a transmission efficiency of 81.07% at optical communication wavelength, 1.55μm. Convenience related to fabrication and decent performance in wide frequency range makes the coupler peerless. The proposed novel design is anticipated to pave the way for a better future in coupler designing.

6.2 Future Works

In future, the first plan we have is to improve our designed coupler of GaAs to a higher efficiency performance. Then, we have the plan to work on other plasmonic devices such as plasmonic diodes, splitters, frequency converter etc. To give more particular view of the planned future works, following list is provided-

- To find more effective performance of the plasmonic coupler by further analysis of the parameters.
- To find newer coupler designs by adding semi elliptical shapes or other new waveguide structures and analyzing the performance.
- To design the coupler with newer materials which will bring higher efficiency.
- To work with newer plasmonic devices i.e. diodes, splitters, frequency converter etc.

References

1. Ozbay, Ekmel. "Plasmonics: merging photonics and electronics at nanoscale dimensions." science 311.5758 (2006): 189-193.
2. Stockman, Mark I. "Nanofocusing of optical energy in tapered plasmonic waveguides." Physical review letters 93.13 (2004): 137404.
3. Pyayt, A. L., Wiley, B., Xia, Y., Chen, A., & Dalton, L. (2008). Integration of photonic and silver nanowire plasmonic waveguides. Nature nanotechnology, 3(11), 660.
4. Min, Changjun, and Georgios Veronis. "Absorption switches in metal-dielectric-metal plasmonic waveguides." Optics Express 17.13 (2009): 10757-10766.
5. Krasavin, Alexey V., and Anatoly V. Zayats. "Silicon-based plasmonic waveguides." Optics express 18.11 (2010): 11791-11799.
6. Sagor, Rakibul Hasan, Md Saiful Islam Sumon, and Mahir Tazwar. "Design and Analysis of a Novel Air Gap–Based Semi-elliptical Nanoplasmonic Coupler." Plasmonics (2019): 1-9.
7. Atwater, Harry A. "The promise of plasmonics." Sci. Am 296.4 (2007): 56-62.
8. Pillai, S. and, and M. A. Green. "Plasmonics for photovoltaic applications." Solar Energy Materials and Solar Cells 94.9 (2010): 1481-1486.
9. Kawata, Satoshi, Yasushi Inouye, and Prabhat Verma. "Plasmonics for near-field nano-imaging and superlensing." Nature photonics 3.7 (2009): 388.
10. Atwater, Harry A., and Albert Polman. "Plasmonics for improved photovoltaic devices." Materials For Sustainable Energy: A Collection of Peer-Reviewed Research and Review Articles from Nature Publishing Group. 2011. 1-11.
11. Gramotnev, Dmitri K., and Sergey I. Bozhevolnyi. "Plasmonics beyond the diffraction limit." Nature photonics 4.2 (2010): 83.
12. A. Taflove and S. C. Hagness, Computational Electrodynamics: The Finite-Difference Time-Domain Method.Boston, MA, USA: Artech House, 2000
13. K. Xiao,J. P.David, andL.D.James,“A three-dimensional FDTD subgridding algorithm with separatedtemporal and spatial interfaces and related stability analysis,”IEEETrans. Antennas Propag., vol. 55, no. 07, pp. 1981–1990, Jul. 2007
14. G.Sunand,C.W.Trueman,“Approximate Crank-Nicolson schemes for the 2-D finite-difference time-domain method for waves,” IEEE Trans. Antennas Propag., vol. 52, no. 11, pp. 2963–2972, Nov.2004
15. J.-P. Berenger, “A perfectly matched layer for the absorption of electro-magnetic waves,” Journal of computational physics, vol. 114, no. 2, pp.185–200, 1994.

16. Z. Bi, K. Wu, C. Wu, and J. Litva, "A dispersive boundary condition for micro strip component analysis using the FD-TD method,"IEEE Trans. Microw. Theory Tech., vol. 40, pp. 774–777, Apr. 1992
17. D. K. Gramotnev and S. I. Bozhevolnyi, "Plasmonics beyond the diffraction limit," Nature photonics, vol. 4, no. 2, p. 83, 2010.
18. Ekmel Ozb**ay**, Plasmonics: Merging Photonics and Electronics at Nanoscale Dimensions
19. Nanoplasmonic couplers and splitters Rami A. Wahsheh, Zhaolin Lu * and Mustafa A. G. Abushagur
20. Surface plasmon resonance in nanostructured metal films under the Kretschmann configuration. Leong et al, J. Applied Physics 106 (2009).
21. Hung-WenLinaWen-HwaHwubMing-DerGer Journal of Materials Processing Technology Volume 206, Issues 1–3, 12 September 2008, Pages 56-61
22. Md. Ghulam Saber, Rakibul Hasan Sagor,"Analysis of cuprous oxide-based ultra-compact nanoplasmonic coupler"
23. Rakibul Hasan Sagor, Md. Ashraful Hoque and Md. Ghulam Saber, "Performance Analysis of Gallium Lanthanum Sulfide and Cuprous Oxide as Nanoplasmonic Couplers"
24. Saiful Islam Sumon, Mahir Tazwar, Rakibul Hasan Sagor and Sakib Mahtab Khandaker "Design and Analysis of a Semi-Elliptical Ultra-Compact Nano-plasmonic Coupler"
25. R. A. Wahsheh and M. A. Abushagur, "Experimental and theoretical investigations of an air-slot coupler between dielectric and plasmonic waveguides, optics express, vol. 24, no. 8, pp. 8237–8242, 2016.
26. G. Veronis and S. Fan, "Theoretical investigation of compact couplers between dielectric slab waveguides and two-dimensional metal-dielectric-metal plasmonic waveguides," Optics Express, vol. 15, no. 3, pp. 1211–1221,2007.
27. D. Pile and D. K. Gramotnev, "Adiabatic and nonadiabatic nanofocusing of plasmons by tapered gap plasmon waveguides," Applied Physics Letters, vol. 89, no. 4, p. 041111, 2006
28. P. Ginzburg and M. Orenstein, "Plasmonic transmission lines: from micro to nano scale with λ /4 impedance matching," Optics express,vol. 15, no. 11, pp. 6762–6767, 2007.
29. Willets, Katherine A., and Richard P. Van Duyne. "Localized surface plasmon resonance spectroscopy and sensing." Annu. Rev. Phys. Chem. 58 (2007): 267-297.
30. Catchpole, KR and, and Albert Polman. "Plasmonic solar cells." Optics express 16.26 (2008): 21793-21800.
31. Steinberger, B., Hohenau, A., Ditlbacher, H., Stepanov, A.L., Drezet, A., Aussenegg, F.R., Leitner, A. and Krenn, J.R., 2006. Dielectric stripes on gold as surface plasmon waveguides. Applied Physics Letters, 88(9), p.094104.

32. Oulton, R. F., Bartal, G., Pile, D. F. P., & Zhang, X. (2008). Confinement and propagation characteristics of subwavelength plasmonic modes. New Journal of Physics, 10(10), 105018.
33. Ginzburg, Pavel, and Meir Orenstein. "Plasmonic transmission lines: from micro to nano scale with λ/4 impedance matching." Optics express 15.11 (2007): 6762-6767.
34. Martyniuk, P. & Antoszewski, J. & Martyniuk, M. & Faraone, L. & Rogalski, Antoni. (2014). New concepts in infrared photodetector designs. Applied Physics Reviews. 1. 041102. 10.1063/1.4896193.
35. Pozar, D.M., 2009. Microwave engineering. John Wiley & Sons.
36. Maier, Stefan Alexander. Plasmonics: fundamentals and applications. Springer Science & Business Media, 2007.